UNITED NATIONS UNIVERSITY
UNU-GTP
Geothermal Training Programme

Orkustofnun, Grensasvegur 9,
IS-108 Reykjavik, Iceland

Reports 2016
Number 38

BOREHOLE GEOLOGY, HYDROTHERMAL ALTERATION AND STRUCTURAL MAPPING OF WELL HE-30, HELLISHEIDI, SW-ICELAND

Erios Naiga Sembatya
Ministry of Energy and Mineral Development,
Directorate of Geological Survey and Mines
P. O. Box 9, Entebbe
UGANDA
eriesembatya@gmail.com

ABSTRACT

Well HE-30 is located in the Hellisheidi high-temperature geothermal field, SW-Iceland. It is a directional production well which was drilled to 2318 m to explore faults at the western margin of the Hengill fissure system as well as to investigate the Reykjafell mini-graben. HE-30 is composed of hyaloclastites (basaltic tuff, basaltic breccia and pillow basalt) and interglacial lavas, occasionally intruded by fine- to medium-grained crystalline basalts. Permeability is provided through faults, formation boundaries and intrusions. Thirteen feed zones were identified in HE-30. Five intrusions were observed and four alteration zones: smectite-zeolite (116 – 456 m), mixed layer clay (456 – 718 m), chlorite - epidote (718 – 1014 m), and epidote – actinolite (1014 – 1328 m). Fluid inclusion homogenization temperatures are lower than in the formation and alteration temperatures, which may indicate an old formation temperature. Alteration and formation temperatures indicate that the system is in thermodynamic equilibrium.

1. INTRODUCTION

Surface exploration surveys, investigation of subsurface geothermal and production characteristics of the reservoir, have to be carried out before utilization of the geothermal field since geothermal systems usually have complicated geology. These include lithology, hydrothermal alteration of the rocks, fluid characteristics such as flow into the system (natural recharge), within the system (fluid convection) and out of the system to the surface (surface manifestations), permeability and hydrological characteristics of the reservoir characteristics. Joint interpretation of the data is then done by various disciplines to decide if the system should be utilized (Steingrímsson and Gudmundsson, 2006). Hengill is an active central volcano located about 30 km southeast of Reykjavik. In the Hengill area there are four main geothermal fields; Hellisheidi, Nesjavellir, Bitra and Hverahlíd (Figure 1) (Franzson et al., 2010). There are over 100 boreholes drilled in Hengill for exploration and production and more than 20 for reinjection (Helgadóttir et al., 2016). A total of 420 MWe electricity and 430 MWt thermal energy are produced from the Hengill geothermal field from three power plants operated by Reykjavik Energy (Hardarson et al., 2015). Well HE-30 was drilled as a production well and to explore faults at the western margin of the Hengill fissure system as well as to investigate the Reykjafell mini-graben. The objective of this

project was to explore the lithology and understand the permeable zones in well HE-30 by locating the fractures and faults in its path and linking them to surface structures.

2. GEOLOGY AND TECTONICS OF ICELAND AND HENGIL

2.1 Geology of Iceland

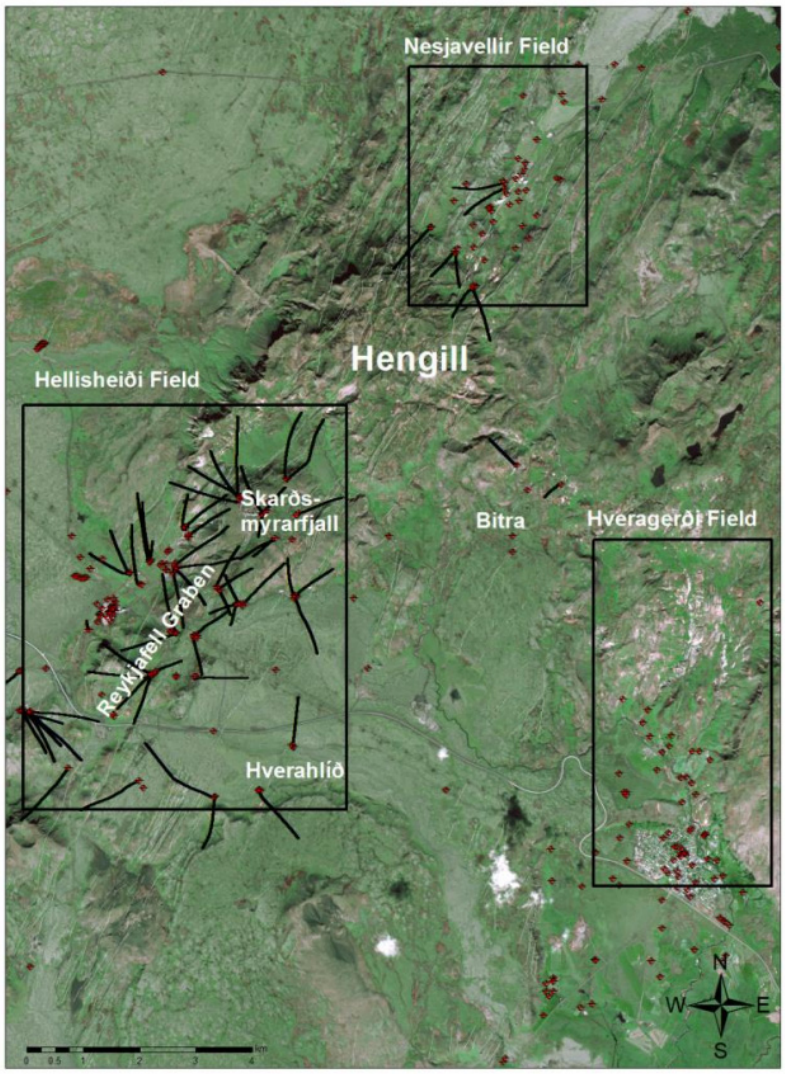

FIGURE 1: Satellite image showing the location of the different fields in the Hengill central volcano and the Reykjafell mini-graben (Hardarson et al., 2015)

Iceland is located on the Mid-Atlantic ridge and above a mantle plume which for about 24 million years has caused intense magmatism and complex tectonism (Hardarson et al., 2015) with sea floor spreading of about 1 cm per year in opposite directions (Saemundsson, 1979). Iceland is composed of three geological formations which date back 16 my (Hardarson et al., 1997). First are the basalt lavas (covering 80-85%) which occur in three types. There is olivine tholeiite which erupted as pahoehoe lava flows, simple tholeiitic flows with little or no olivine which erupted as aa fissure lavas and the porphyritic flows with plagioclase and/or pyroxene which formed in fissures as thick and massive flows. Second are the acidic lavas with intermediate rocks (which cover 10%) of which 60-70% are lavas and intrusions. There are dolerite, gabbro and granophyre that are exposed in the eroded central volcanoes, then 30-40% being pyroclastites deposited in and around vents as ash flows or tuff sheets and transported over long distances (Figure 2). Third (5-10%) are the alkaline rocks found in the neovolcanic zones underlain by the tertiary tholeiites. There are four stratigraphic series based on climatic evidence (Figure 2) (Saemundsson, 1979). *Tertiary rocks* were formed more than 3.1 my ago and cover half of Iceland or about 50,000 km^2. They vary in lithology from the tholeiitic lavas to intermediate and acidic rocks. The *Plio-pleistocene lavas* were formed around 0.7 – 3.1 my ago and cover 25,000 km^2. They are made up of tillites interstratified with pillow lavas, various types of breccia and hyaloclastites. The *Upper Pleistocene* lavas were formed about 0.7 my ago. They are marked by an unconformity with the Plio-pleistocene lavas. During their eruption, they covered the fissure swarms forming table mountains. They occur in central, western and south western Iceland. From their structure and morphology, they were classified into two types, the grey basalts erupted during interglacial periods and the subglacial

palagonites (pillow lavas and hyaloclastite tuffs). Lastly to mention are the *Postglacial lavas* (less than 12,000 years old) which occur in the active rift zones of Iceland. They cover 12000 km^2 (10%) of Iceland and are 90% basalts and 10% intermediate and acidic lavas (Saemundsson, 1979).

2.2 Tectonics of Iceland

Neovolcanic zones together with the graben structures, oblique and transverse fissure zones are tectonically active unlike the Tertiary and Pleistocene zones except where younger tectonic zones cross cut them (Saemundsson, 1979). The axial rifts in the neovolcanic zones, where active plate growth occurs, mainly erupt tholeiitic rocks and fracturing is localized in fissure swarms. Volcanic fissures, non-eruptive gaping cracks and faults are the dominant structures in these swarms and they are associated with dyke injection, as seen in the old lava piles (Saemundsson, 1979). These dykes are 1-20 m wide and can be several km long. Central volcanoes host most fissure swarms. These fissure swarms are about 10-30 km wide and 50-100 km long. Sometimes narrow grabens are found within the fissure swarms, for example the Mt. Reykjafell mini-graben (Figure 3). The volcanoes sometimes form calderas with about 5-10 km diameter, which in turn, develop cone sheets stretching beyond caldera margins (Saemundsson, 1979). Transforms and seismic zones are zones where active strike-slip tectonic activities occur. These include the South Iceland Fracture Zone (SIFZ) and the Tjörnes Fracture Zone (TFZ). The largest earthquakes in Iceland occur along these transforms (Figure 2).

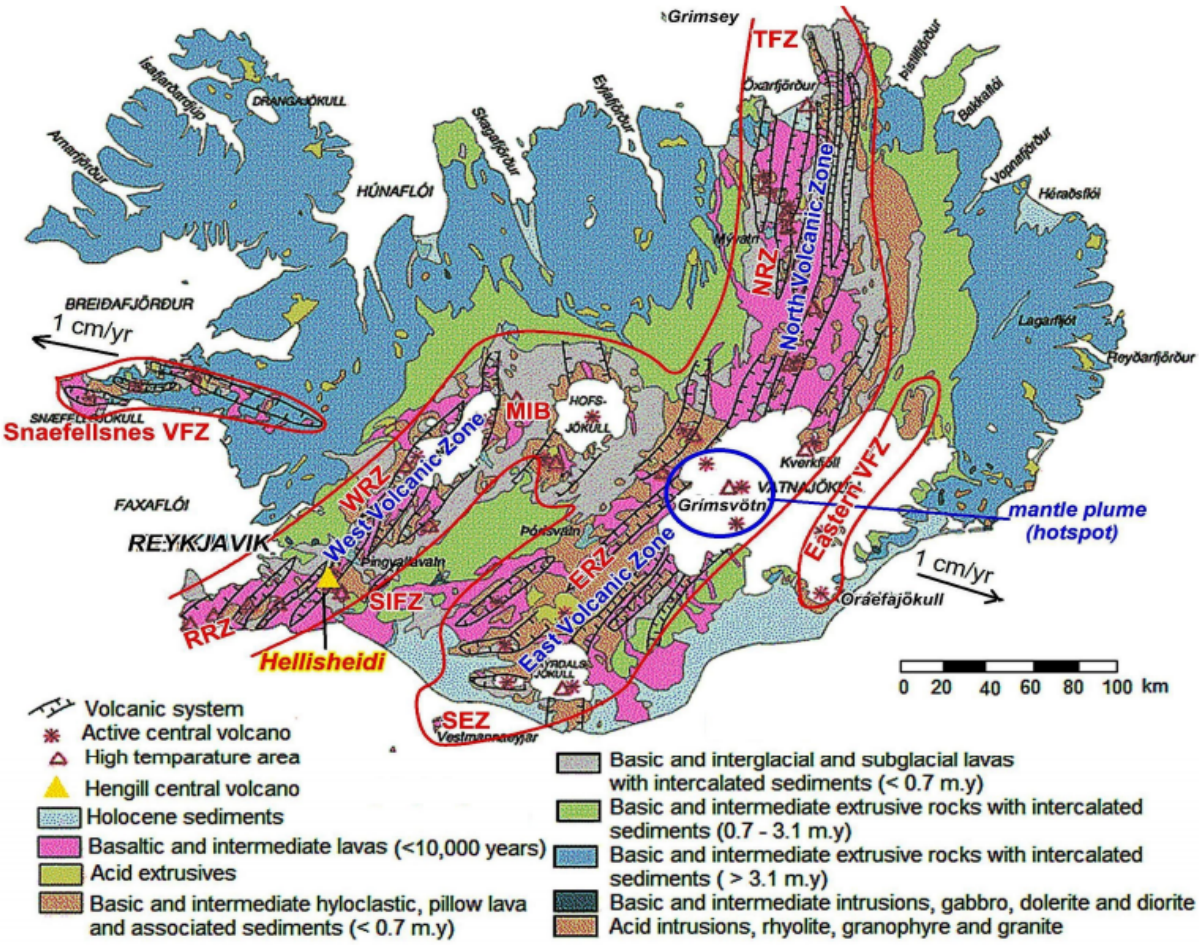

FIGURE 2: Map of Iceland showing the volcanic systems and fissure swarms, location of the mantle plume, rift systems, direction of spreading and location of the Hellisheidi high-temperature geothermal field in the Hengill central volcano (modified from Saemundsson, 1979; Bawasu, 2010)

2.3 Hengill geology and structural setting

2.3.1 Geology of Hengill central volcano

Hengill volcano is about 400,000 years old. The highlands (about 800 m a.s.l.) are covered by hyaloclastites that erupted during the glacial periods and the interglacial lava flows, which are found in the lowlands (Franzson et al., 2010). Hyaloclastites are comprised of pillow basalts, breccia and tuff, which have high porosity but low permeability when altered (e.g. Gebrehiwot Mesfin, 2010). Three volcanic systems are found in the area. One is called the Hveragerdi-Grensdalur volcanic system, which is no longer volcanically active but is seismically. Here the oldest rocks are found (about 0.8 my). The other two systems are the Hrómundartindur volcanic system with rocks younger than 0.2 my and the Hengill volcanic system which is still active (e.g. Gebrehiwot Mesfin, 2010). Hengill is a complex volcano with a fissure swarm that is 5 – 10 km wide and 40 - 60 km long (Franzson et al., 2010; Hardarson et al., 2015). The main fractures trend NNE-SSW. Other structures strike N-S and WNW-ESE (Árnason, 2007; Spichak et al., 2013). Hellisheidi is a high-temperature field found in the Hengill central volcano (Figures 1 and 2). It is located at the intersection of the Western Iceland volcanic zone (an axial rift zone), the Reykjanes Peninsula (an oblique spreading ridge), and the South Iceland seismic zone (a seismically active transform zone). This triple junction of the American-Eurasian plate boundary has been described by Hardarson et al. (2015) and Gasperikova, et al. (2015).

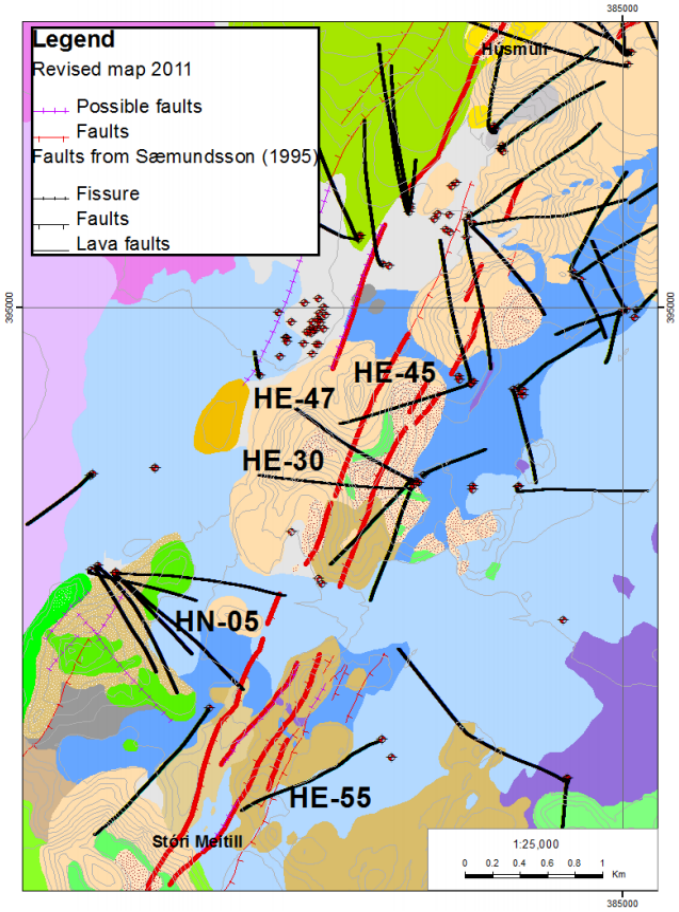

FIGURE 3: Map showing the Reykjafell mini-graben (red lines) (Hellisheidi field) which is located on the western flank of the Hengill fissure swarm. It strikes NE-SW, through Mt. Reykjafell, and wells that penetrate the Reykjafell mini-graben are very productive (about 10 MW). Postglacial lavas (<12000 years) are drawn in blue-purple, subglacial hyaloclastites in brown and interglacial lavas in green (Hardarson et al, 2015)

2.3.2 Hengill structural setting

Reykjafell mini-graben: Several geological surveys have been conducted in this area including a detailed surface mapping of the Mt. Reykjafell mini-graben (Figure 3), which transects Mt. Reykjafell towards the southwest, covering the Gráuhnúkar area, Mt. Stóri Meitill and Mt. Litli Meitill (Hardarson et al., 2015). There are a number of surface manifestations on the eastern rim of the graben. South of Mt. Reykjafell and the subglacial craters that are >10,000 years old, striking NE to SW additionally to some others which are within the graben (Gunnarsdóttir, 2012). The Reykjafell mini graben probably extends northeast towards Nesjavellir (Hardarson et al., 2015). It trends NNE-SSW with a 20-40 m down-throw on the surface and are 150-400 m wide (Hardarson et al., 2015). Three volcanic fissure swarms erupted after the last glaciation or about 9,000, 5,000 and 2,000 years ago (Figure 4). Permeability is provided by formation boundaries, intrusions, faults and feeder dykes in the Hengill volcano (Franzson et al., 2010; Gasperikova et al., 2015). Holocene

volcanic fissure eruptions have increased the permeability and geothermal activity in the volcano. This was confirmed by the renewed heating in the Nesjavellir geothermal filed by the fissure swarms which are 5,000 and 2,000 years old (Figure 4). The Reykjafell mini graben provides up-flow zones as has been confirmed by geophysical data (Hardarson et al., 2015). Analysis of drill cuttings and drill data was done to understand the subsurface and indicates that the wells which penetrate the graben and its faults have an output of >10 MWe and also show a down throw of greater than 200 m at 1300 m depth (Hardarson et al., 2015).

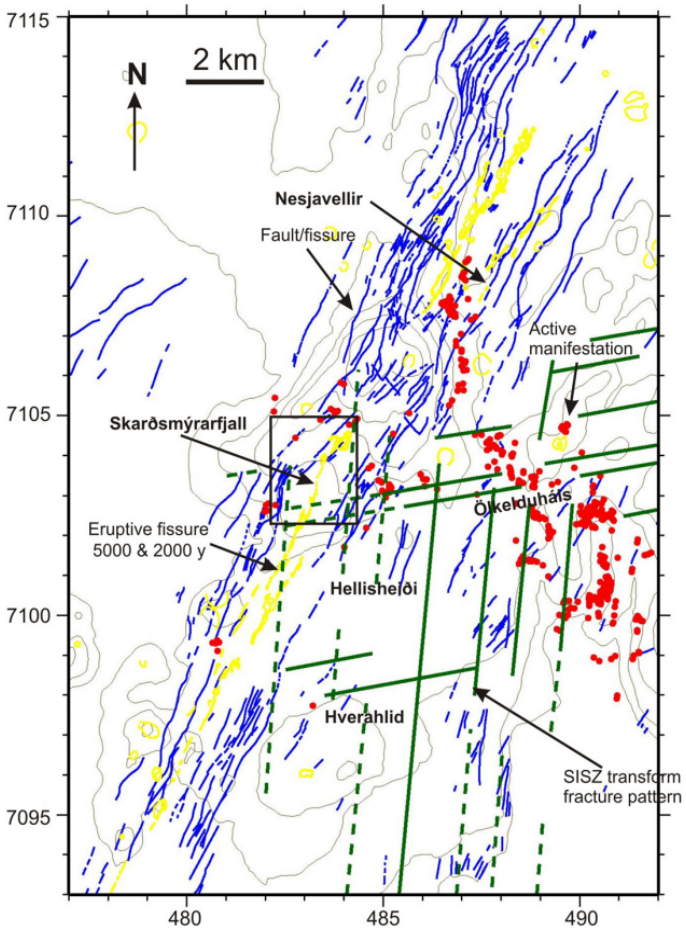

FIGURE 4: The Hengill volcanic system. Red dots tag surface manifestations, blue lines indicate surface fissures and faults, fissures and faults defined by earthquake locations are sketched in green and yellow lines mark postglacial fissures (Franzson, et al., 2010)

3. LITERATURE REVIEW ON HENGILL GEOTHERMAL FIELD

Work has been ongoing in Hengill central volcano since 1975 including surface exploration surveys such as geological, geochemical and geophysical exploration, TEM/MT surveys, borehole resistivity measurements, subsurface geology analysis and hydrothermal alteration mapping (Haraldsdóttir et al., 2015). Worldwide, there is a similarity in the responses of resistivity and P-wave velocities at temperatures below 350°C (e.g. Gasperikova et al., 2015). Resistivity survey results show that the Hengill volcano has a high-temperature geothermal source. Relating resistivity, well temperatures and alteration mineralogy show that the resistivity features in the volcano is more dependent on the hydrothermal mineral alteration than the temperature (e.g. Gasperikova et al., 2015). When a geothermal system cools, alteration minerals that remain indicate the maximum temperatures when these minerals were formed (Haraldsdóttir, et al., 2015). Both the resistivity and reservoir models indicate similar results (Björnsson and Hersir, 1981). Figure 5 shows low resistivity in the first 1-2 km which is due to the smectite-zeoloite zone and mixed layer clays formed at temperatures <200°C. This zone is called the clay cap, which is caused by the conductivity of loosely bound cations in smectite and zeolite minerals (Haraldsdóttir, et al., 2015). Underneath is a high resistivity core caused by chlorite and other alteration minerals that are compacted and with little water, like epidote which forms at temperatures >250°C (Haraldsdóttir et al., 2015). Another low resistivity anomaly is found at even greater depth. The eruption in Bitra geothermal system about 13,000 years ago re-activated this system that had cooled during the glacial period (e.g. Gasperikova et al., 2015). Microearthquakes are common in Hengill volcano because of its location and they are linked to the geothermal surface manifestations (e.g. Gebrehiwot Mesfin, 2010). This is indicated by the dense fissure swarm and recent eruptions (e.g. Hardarson, 2014). These occur at about 5 km depth, and strike E-W or N-S. Seismological surveys revealed two seismic vibrations, the infrequent and intense earthquakes caused by movement of the crust as a result of release of stress along plate boundaries and the small quakes in the Hveragerdi central volcano (e.g. Gebrehiwot Mesfin, 2010).

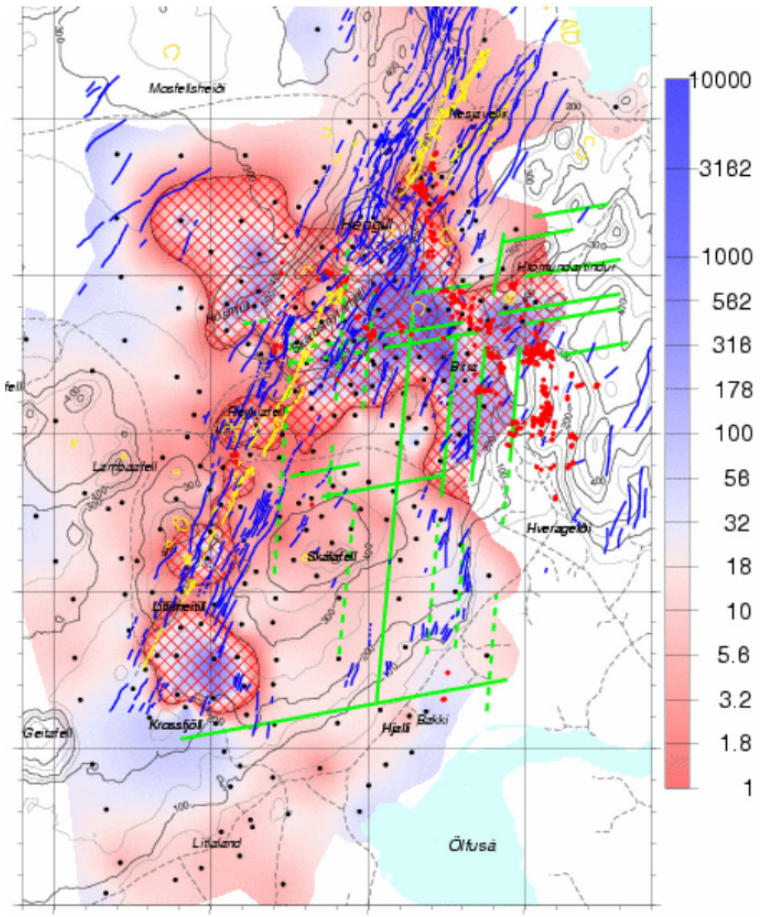

FIGURE 5: Map showing resistivity variations in Hengill central volcano at 850 m b.s.l., high resistivity cores (cross-hatched) below low resistivity indicate alteration temperatures above 230°C, surface geothermal springs (red dots), fissures (blue lines) and faults (green lines)earthquake locations and post glacial (< 12 ka) fissures (yellow lines) (Árnason, 2007)

4. BOREHOLE GEOLOGY

4.1 Drilling of HE-30

The drilling of HE-30 was carried out in four phases during February and March 2007. Drilling depths, casing depths and drill bits in well HE-30 are presented in Table 1. The well path according to gyro surveys is shown in Figure 3. The well was drilled using the rig Ódinn Drillmec HH-220 series. Well HE-30 was spudded on the 20th of February 2007 and was completed on the 48th working day, April 4th. Pre-drilling with a 26" drill-bit commenced on the 5th working day, and drilling down to 91 m depth was completed in one day. The well was cased with 22½" pipes (surface casing) to 90.7 m depth and cemented using 20.5 m^3 of cement slurry. Phase one, when a 21" bit and motor was used, started on February 26th and was completed, at a depth of 300 m, late in the evening of the following day. The well was cased with 18⅝" pipes (anchor casing) down to 300 m. Subsequently 28 m^3 of cement slurry was used to set the casing. No circulation losses were encountered during pre-drilling and phase one. Phase two commenced on March 3rd using a 17½" bit, motor and MWD (Measurement While Drilling) in the BHA (Bottom Hole Assembly). The well was drilled to 707 m and cased with a 13⅜" production casing, which was set at 705 m depth and cemented with 71 m^3 of slurry. The well design assumed a KOP (Kick Off Point) at 320 m with a 2.5°/30 m build-up reaching the final inclination of 30° at 690 m depth. The direction was 270° west. Gyro surveys showed that by the end of phase 2 the inclination was 30.8° and azimuth 268° which are very acceptable results. Phase three commenced on March 16th on workday 29 and a 12¼" bit was used. Aerated drilling with foam and water was chosen. The well was drilled to 2318 m and the 9 ⅝" slotted liner extends to a depth of 2256.5 m. There was loss of circulation at 1288 m (Gunnarsdóttir, 2012). Total loss of circulation occurred at 1328 m and no drill cuttings were retrieved below that depth. Well HE-30 was completed on April 4th on workday 48.

TABLE 1: Drilling depth, casing depth and drill bits in well HE-30. Depths refer to the platform of Ódinn, 6.7 m above ground level (Hardarson et al., 2007a, 2007b)

Rig	Drill Phase	Drill bit	Drill depth	Casing	Casing depth
Ódinn	Pre-drilling	26"	91 m	22 ½"	90,7 m
Ódinn	1. Phase	21"	300 m	18 ⅝"	300 m
Ódinn	2. Phase	17 ½"	707 m	13 ⅜"	705 m
Ódinn	3. Phase	12 ¼"	2318 m	9 ⅝"	2256,5 m

4.2 Methodology

Binocular microscope: A total of 606 drill cutting samples from 0 to 1328 m depth, which were sampled at a 2 m depth interval, were analysed in detail to determine rock type, alteration, oxidation, intrusions, fractures and vein fillings. Lithological and alteration logs were prepared.

Petrographic analysis; In well HE-30, 21 thin sections from the first 1278 m were analysed to provide a detailed description of the rock including mineral type, texture, fractures, porosity, alteration minerals and alteration sequences (Table 3).

X-ray diffractometer (XRD) analysis: Clays were not easily distinguished by binocular and petrographic microscopes. A X-ray diffractometer was used to analyse clays to delineate the alteration zones which aided the interpretation of alteration temperatures in the geothermal field. Three categories of samples were analysed (at Icelandic GeoSurvey – ISOR): untreated, treated with the glycol solution and heated samples. Sample preparation was done for 24 to 48 hours before placing the samples in the XRD for measurement. Twenty-two samples from the first 1282 m depths in HE-30 were analysed and the results indicate smectite, chlorite, illite (minute amount) and mixed layered clays.

Fluid inclusion analysis: Fluid inclusions (FI) are bubbles of liquid or gas trapped in a crystal. The inclusion may be primary (formed during crystal growth) or secondary (formed after crystal growth), pseudosecondary inclusions exist as well but are not used in this analysis. FI were used to understand the thermal evolution of the geothermal system by carrying out microthermometric analysis where they are used as geothermometers to measure the homogenization temperature (T_h) (Shepherd et al., 1985; Bodnar, 2003) by heating quartz and calcite crystals, which contained the inclusions until the trapped bubble(s) disappeared. The maximum temperature was recorded which gives an estimate of the temperature at the time of the mineral formation.

4.3 Lithology of well HE-30

HE-30 is composed of fine- to medium-grained crystalline basalts (postglacial/interglacial lavas and intrusions) and hyaloclastites (tuff, breccia and pillow lavas). They were identified by their physical properties such as grain size, minerals and crystal shape, colour, extent of alteration, alteration minerals and oxidation and many other factors were noted using a binocular microscope. The results are summarised in Figure 6.

0 – 12 m: No cuttings.

12 – 48 m: Fine- to medium-grained crystalline basalt; Greyish brown fine- to medium-grained crystalline basalt with phenocrysts of plagioclase, pyroxene and olivine. Samples from 14 -16 m and 22-26 m were slightly oxidized thus indicating the presence of magnetite in them. At 18m, 34 – 38 m and 46 – 48 m there were few scattered pores filled with calcite.

48 – 58 m: Glassy basalt (Pillow basalt); Porous brownish fine- to medium-grained pillow lava with calcite and silica in vesicles. Plagioclase, pyroxene and olivine phenocrysts with some calcite were observed.

58 – 70 m: Basaltic tuff; Greyish to dark coloured fine- to medium-grained tuff with plagioclase, pyroxene and olivine phenocrysts. 60 – 66 m had patches of fresh glass. 66 – 70 m were highly fractured and veins were filled with calcite.

*70 – 80 m: Fine- to medium-grained crystalline basalt; D*ark grey fine- to medium-grained microcrystalline olivine tholeiite with plagioclase and pyroxene phenocrysts. 78 m was highly fractured, veins were filled with calcite.

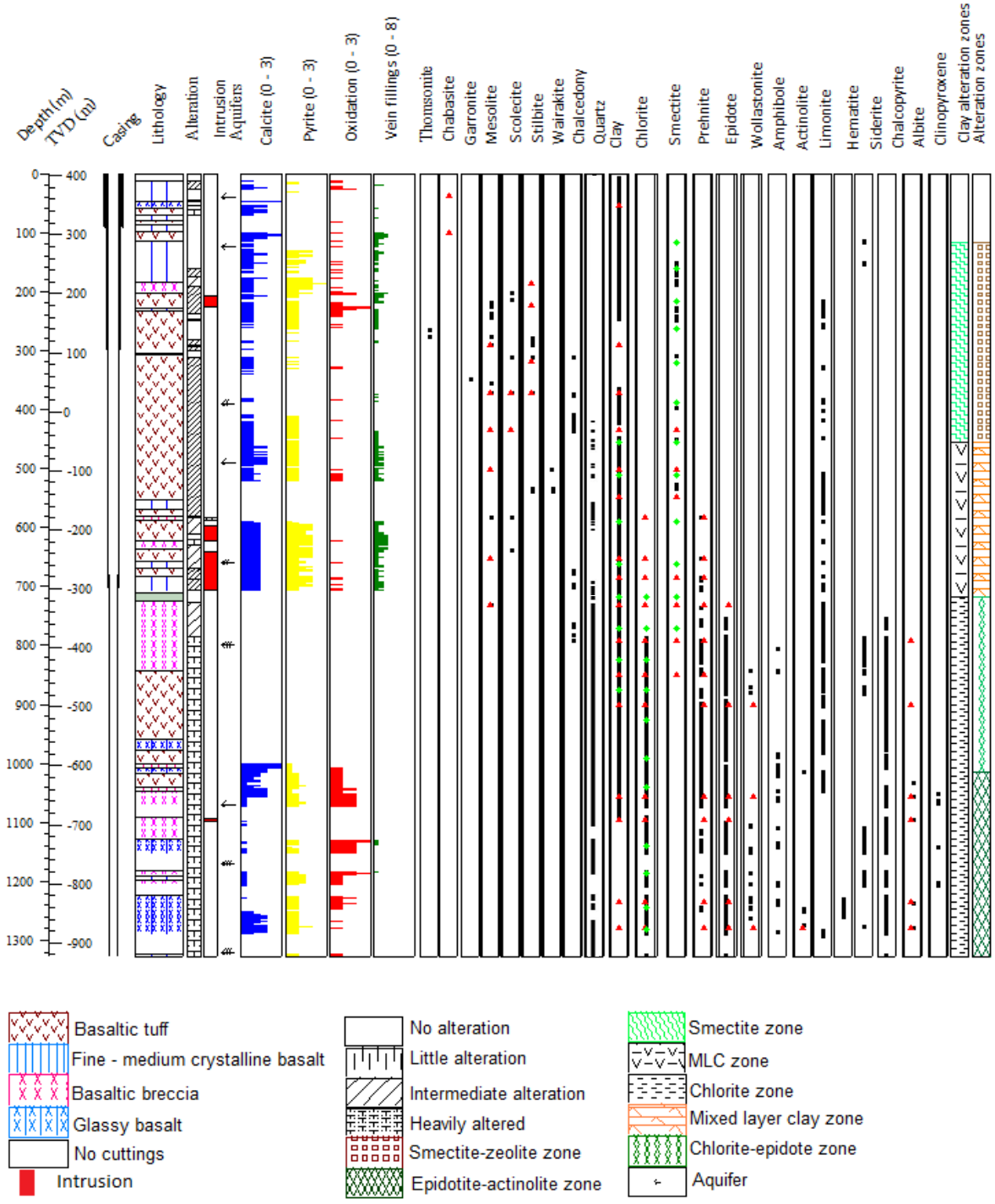

FIGURE 6: Lithology, alteration mineral distribution, intrusions, aquifers and alteration zones of well HE-30 from 0 to 1328 m;
◆ XRD analysis, ▲ petrographic analysis and ∎ binocular analysis

80 – 86 m: Basaltic tuff; Very porous greyish brown tuff. Slight oxidation observed at 82 m, thus limonite is present. There was occurrence of fresh scoria.

86 - 98 m: Fine- to medium-grained crystalline basalt with cement.

98 – 114 m: Basaltic tuff; 98 – 110 m samples were highly fractured greyish tuff with few pores. Cuttings at 110 – 114 m were crystalline, slightly fractured and oxidized with presence of siderite, limonite and less glass. The veins were filled with silica and calcite.

114 – 184 m: Fine- to medium-grained crystalline basalt; Slightly fractured fine- to medium-grained olivine tholeiite. It is slightly oxidized in the first 10 metres with silica and calcite in the veins. 136 – 138 m were more fractured. The lower part was porous with plagioclase and pyroxene phenocrysts and clay, calcite and pyrite filled the vesicles. Pyrite appeared at 128 m.

184 - 204 m: Basaltic breccia; Very porous greyish brown basaltic breccia with phenocrysts of plagioclase and olivine. It is slightly oxidized resulting into limonite. There was occurrence of calcite and pyrite, vesicles and quartz and scolecite in veins.

204 – 228 m: Basaltic tuff with scoria; Highly fractured greyish to dark brown crystalline basaltic tuff with olivine and plagioclase phenocrysts. Scoria was observed in this rock. The rock was intruded by a dark grey, less altered, fine-grained crystalline basalt. The secondary minerals were chabazite, stilbite and limonite. Veins were filled with calcite and pyrite with clays forming a thin lining in the vesicles.

228 – 234 m: Pillow basalt; Highly fractured and slightly oxidized dark grey to black crystalline pillow basalt with olivine, pyroxene and plagioclase phenocrysts. There was presence of amorph silica, smectite, limonite, calcite, and pyrite, veins were filled with calcite. Grains from a fine- to medium-grained crystalline basalt intrusion were also observed.

234 – 240 m: Fine- to medium-grained crystalline basalt; Fractured, less oxidized and less altered dark grey fine- to medium-grained crystalline basalt with phenocrysts of olivine, plagioclase and pyroxene. Secondary minerals were chabazite, mesolite, quartz, smectite with calcite and pyrite filling the veins.

240 – 300 m: Basaltic tuff; Porous greyish brown crystalline basaltic tuff with phenocrysts of plagioclase and pyroxene. 240 – 262 m and 284 – 286 m were fractured with calcite, pyrite and quartz in the veins. Smectite, mesolite, quartz and calcite filled some pores. It was slightly oxidized thus presence of magnetite and limonite was indicated.

300 – 304 m: No cuttings.

304 – 308 m: Basaltic breccia; Brownish crystalline basaltic breccia with abundant cement.

308 – 554 m: Basaltic tuff; Greyish brown, fairly fractured and slightly oxidized (presence of limonite) basaltic tuff with little cement in the upper part. It is crystalline and very fine in the middle and highly fractured at the bottom. There were no cuttings at 494 m and 498 m depths. Wairakite, chalcedony, calcite, and pyrite were observed in the vesicles and the veins were filled with quartz, calcite and pyrite. There were numerous grains of fine- to medium-grained crystalline basalt.

554 – 570 m: Fine- to medium-grained crystalline basalt; Fractured and altered rock with phenocrysts of plagioclase and numerous calcite and pyrite grains. The bottom was oxidized thus showing limonite. There were sedimentary grains and calcite in veins.

570 – 582 m: Basaltic tuff; Fractured and oxidized (limonite shown) brown crystalline basaltic tuff with olivine phenocrysts. There were calcite and pyrite grains in veins and vesicles. No cuttings could be retrieved from 582 m.

582 – 588 m: Tuffrich breccia; Very altered and fractured dark grey to greyish tuffrich breccia which was intruded by dark coloured compact fine-grained crystalline basalt (possible intrusion). Calcite and pyrite filled the vesicles and veins.

588 – 622 m: Basaltic tuff; Highly fractured and very altered greyish brown basaltic tuff with phenocrysts of pyroxene, abundance of calcite and pyrite grains in vesicles and in veins. It was intruded by a fresh dark grey fine-grained crystalline basalt, probably a dyke. 620 – 622 m were slightly oxidized (presence of limonite).

622 – 636 m: Basaltic breccia; Very altered and highly fractured greyish brown basaltic breccia. It had abundant calcite and pyrite grains, quartz, calcite and pyrite in veins. Fresh dark grey fine-grained crystalline basalt, probably a dyke intrusion was seen throughout this rock.

636 – 658 m: Basaltic tuff; Very altered and fairly fractured greyish brown basaltic tuff with calcite and pyrite grains and scolecite, quartz and calcite in veins. Prehnite was observed in the tuff. An intrusion of fresh dark grey fine-grained crystalline basalt, probably a dyke, was also observed in this rock.

658 - 668 m: Fine- to medium-grained crystalline basalt; Very altered and fairly fractured dark grey crystalline basalt (olivine tholeiite) with calcite and pyrite grains and in veins. An intrusion of fresh dark grey fine-grained crystalline basalt, probably a dyke, is also observed in this rock.

668 -684 m: Basaltic tuff; Very altered and fractured fine-grained brownish basaltic tuff which was intruded by a fresh and compact dark grey fine-grained crystalline basalt, with phenocrysts of plagioclase and olivine. There was chalcedony, quartz, abundance of calcite and pyrite in the veins. 682 – 684 m were slightly oxidized showing limonite.

684 – 707 m: Fine- to medium-grained crystalline basalt; Altered, fractured and slightly oxidized (showing limonite) dark grey grained crystalline basalt (olivine tholeiite) with phenocrysts of plagioclase and pyroxene. Chalcedony, quartz, abundance of calcite and pyrite was observed in the veins. There was a dyke intrusion present.

707 – 712 m: No cuttings.

712 – 724 m: Cement.

724 – 844 m: Basaltic breccia; Altered, slightly oxidized and more fractured greenish brown to dark grey very fine-grained rock with some epidote. The samples from 788 – 844 m were more altered. There was prehnite at 818 – 820 m. Calcite, chalcopyrite and quartz were observed in the veins while in the vesicles, there was chalcedony, calcite, quartz, chlorite, chalcopyrite, epidote and prehnite.

844 – 958 m: Basaltic tuff; Very altered, oxidized (presence of siderite and limonite) and highly fractured greenish grey rock with less calcite and chalcopyrite. Calcite, chalcopyrite and quartz were observed in veins while chalcedony, calcite, quartz, chlorite, chalcopyrite, epidote and prehnite were observed in vesicles. Other secondary minerals included wollastonite.

958 – 978 m: Pillow basalt; Very altered and slightly oxidized dark to grey coloured rock with quartz, chlorite, calcite, chalcopyrite and epidote filling the vesicles. Other secondary minerals were prehnite, and siderite.

978 – 1000 m: Basaltic tuff; Very altered greenish grey and very fine-grained tuff with a lot of calcite and less chalcopyrite. Other minerals that were observed here were prehnite, epidote, quartz and amphibole.

1000 – 1008 m: Tuff-rich breccia; Very altered dark grey to greyish tuff-rich breccia with abundance of calcite and to a smaller extent chalcopyrite. Quartz, amphibole, prehnite and epidote were observed in this rock.

1008 – 1018 m: Pillow basalt; Very altered and slightly oxidized (limonite shown) pillow basalt with more calcite and less chalcopyrite. Other secondary minerals that were observed were chlorite, epidote, prehnite and amphibole.

1018 – 1040 m: basaltic tuff; Very altered and slightly oxidized (limonite shown) greenish brown tuff. There was less chalcopyrite and calcite. Other secondary minerals that were observed were chlorite, epidote, prehnite and amphibole.

1040 – 1048 m; Tuff-rich breccia; Very altered and oxidized dark grey to greyish rock with more calcite and less chalcopyrite. Chlorite, prehnite and epidote were also seen.

1048 – 1072 m: Basaltic tuff; Very altered and very oxidized microcrystalline greenish grey to dark aphyric basaltic breccia. 1040 – 1048 m has more calcite than the bottom part. Chalcopyrite, chlorite, quartz and prehnite were observed.

1072 – 1092 m: No cuttings.

1092 – 1128 m: Basaltic breccia; Very altered greenish breccia with traces of calcite at the bottom. At 1094 – 1098 m, it was intruded by dark grey fine-grained crystalline basalt that was fresh and compact.

1128 – 1152 m: Pillow basalt; Very altered and oxidized greyish black pillow basalt with pyroxene phenocrysts. Few traces of calcite were observed at the bottom and 1130 – 1138 m were fractured. Secondary minerals observed were quartz, chalcopyrite, chlorite, epidote, siderite, prehnite, wollastonite and amphibole. There were several crystals of wollastonite at 1144 m.

1152 – 1182 m: No cuttings.

1182 – 1192 m: Basaltic breccia; Very altered and much oxidized greyish brown, fine material of basaltic breccia with abundance of epidote in the upper part and with phenocrysts of pyroxene and olivine at the bottom. Quartz, calcite (few traces), epidote, chlorite, chalcopyrite, prehnite, wollastonite and siderite were the secondary minerals that were observed. A vein in 1184 m was filled with quartz and epidote.

1192 – 1198 m: Fine- to medium-grained crystalline basalt; Very altered and fairly oxidized dark coloured aphyric crystalline basalt with few traces of calcite. Quartz, epidote, chlorite, chalcopyrite and siderite were the secondary minerals that were seen.

1198 – 1208 m: Basaltic breccia; Very altered greyish brown very fine material of basaltic breccia with abundance of epidote and quartz and less calcite and chlorite. It was slightly oxidized and the other secondary minerals include siderite, quartz, chalcopyrite, prehnite, amphibole and wollastonite.

1208 – 1224 m: No cuttings.

1224 – 1288 m: Basaltic breccia; Very altered and much oxidized greenish grey pillow basalt which was aphyric with abundance of chlorite, quartz and epidote. There was not any chlorite at the bottom (1282 -1288 m). Other secondary minerals observed were wollastonite, actinolite, amphibole, prehnite, siderite and chalcopyrite. Traces of calcite were seen at 1228 m.

1288 –1324 m: No cuttings.

1324 – 1328 m: Pillow basalt; Very altered and slightly oxidized, greyish black aphyric pillow basalt with a lot of quartz and epidote and little chlorite. Actinolite was observed as well as chalcopyrite and siderite.

No further cuttings were retrieved from the well due to total loss of circulation.

4.4 Intrusions

Intrusion are usually compact with oxidized margins. They can be indicators of good permeability. In HE-30, these intrusives were observed in the cuttings, using a binocular microscope, as dark grey fine- to medium-grained microcrystalline basalts (Figure 6). Oxidation was observed at 208-226 m and at 528-588 m. Peaks were observed in the neutron log at 598-622 and 642-707 m. Another peak was observed at 1094-1098 m in the resistivity curve (Hardarson et al., 2007a; 2007b; Gunnarsdóttir, 2012). Figure 7, as obtained from leapfrog; shows HE-30 intercepting the intrusions (642-707 and 1094-1098 m) and faults.

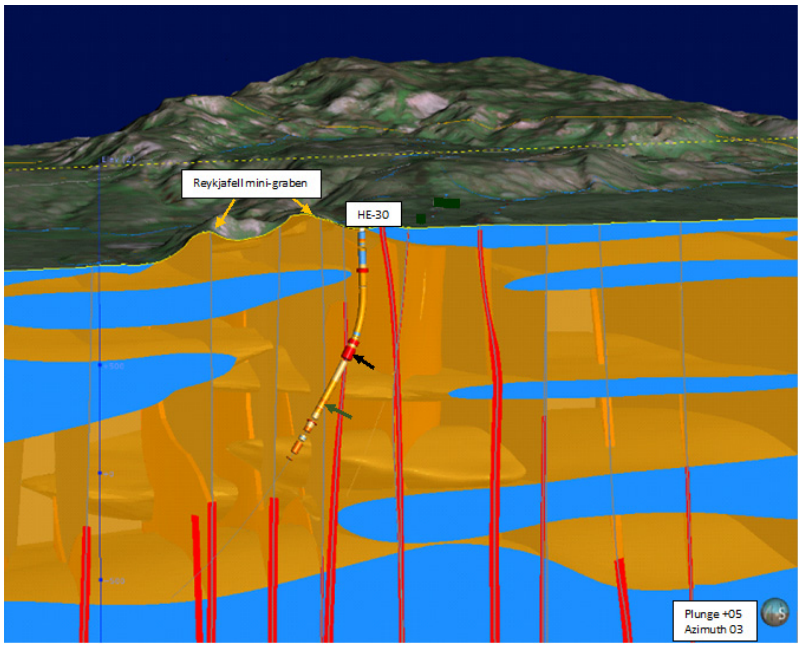

FIGURE 7: Path of well HE-30, fine – medium crystalline basalt (blue), hyaloclastites (yellow), intrusions in Hellisheidi field (red), faults (light blue), Reykjafell mini-graben (yellow arrows) and intrusion in HE-30 at 632 – 707 m (black arrow) and 1094 – 1098 m (dark green arrow)

4.5 Aquifers / feed zones

Thirteen feed zones were observed from temperature logs (Figure 8). They are at 40, 125, 390, 490, 660, 800, 1070, 1170, 1310, 1460, 1550, 1680 and 1960 m depth. The aquifers in the zones of loss of circulation (Figure 6) are in 1070, 1170 and 1310 m depth while 490 and 1070 m had abundance of calcite and pyrite which indicates permeability. There was total loss of circulation below 1328 m. Temperature logs showed that there are feed zones at 1460, 1550, 1680, and 1960 m depth. There are no details on the circulation losses on Figure 8 which shows small aquifers located at 40, 125 and 490 m, medium ones at 390, 660, 1460, 1680 and 1960 m and largest ones at 800, 1070, 1170, 1320 and 1550 m.

4.6 Alteration mineralogy

Minerals that crystallize from magma are called primary minerals (rock forming minerals) while those that result from deposition from geothermal activity and from hydrothermal reactions and/or hydrothermal alteration in host rock inside amygdales, vesicles and fissures are called secondary minerals (Reyes, 2000). Primary minerals alter when subjected to different conditions like temperature, pressure, fluid composition and many more. HE-30 is composed of hyaclastites and basalts with the primary minerals being volcanic glass, olivine, plagioclase, pyroxene and opaque minerals.

4.6.1 Primary minerals

Below is the description of the primary minerals with their alteration products (Figure 9). *Glass:* Glass forms when magma cools rapidly. It is translucent, unstable and easily altered with vitreous lustre and conchoidal fractures. It alters to clay, calcite, zeolites and quartz. *Olivine:* When magma solidifies, olivine crystallizes first. In HE-30 these were small (a few millimetres) yellowish green crystals with indistinct cleavage and conchoidal fractures. It alters to clay, calcite, zeolites and quartz. *Plagioclase:* The most common primary mineral was the calcium rich feldspar with phenocrysts that occurs singly or as clusters. The crystals are white to colourless, flat, columnar or granular and have parallel cleavage,

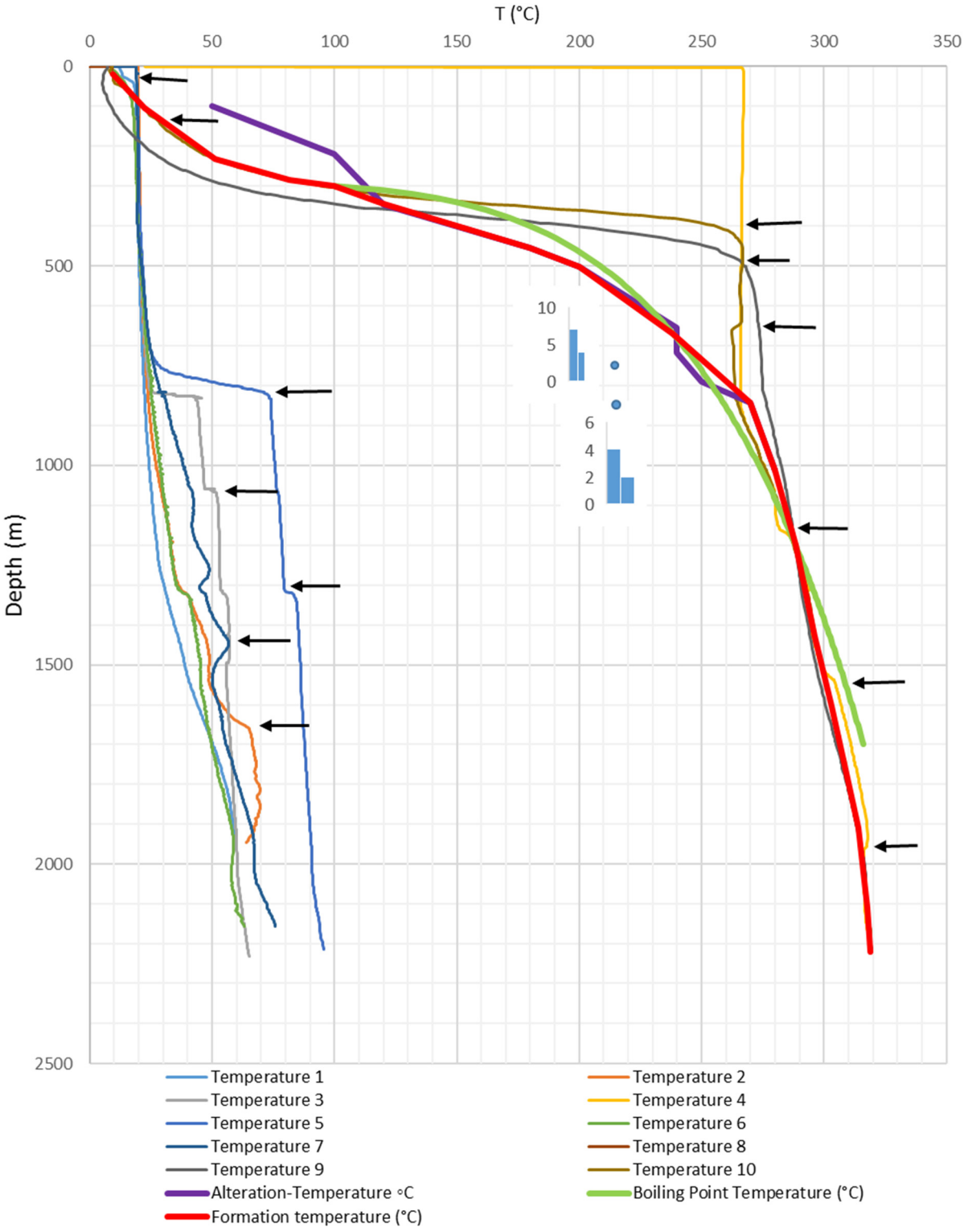

FIGURE 8: Location of feed zones from 0 to 1960 m in HE-30 based on temperature logs at different times in the well including heating-up curves, alteration temperature, formation temperature and homogenization temperature (T_h) (blue dots)

oscillatory zoning and polysynthetic twinning with a low relief (Saemundsson and Gunnlaugsson, 2010). Plagioclase is observed throughout well HE-30. It was altered to albite, wairakite, chlorite and epidote. *Pyroxene:* These were very small black to dark green prismatic crystals of augite. The cleavage was perfect (parallel cleavage) with vitreous lustre observed throughout the well. It was altered to clay,

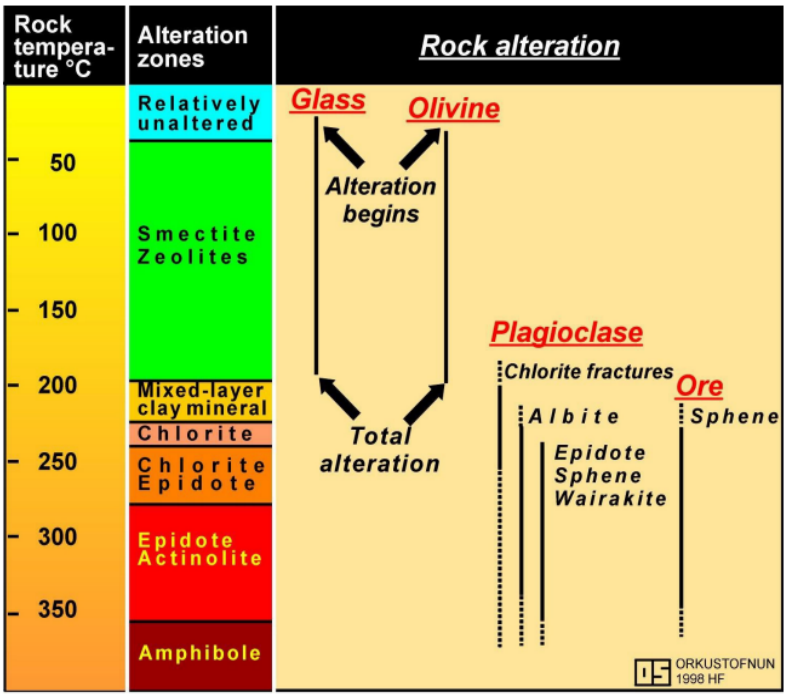

FIGURE 9: Alteration temperatures of primary minerals (Franzson, 1998)

calcite, quartz, chlorite, chlorite, epidote and actinolite. *Opaque minerals:* They were dark coloured and opaque and encountered throughout the well. *Magnetite* occurred as very tiny black cubic crystals with a metallic lustre and precipitated in vesicles or fractures. It was altered to limonite and siderite.

4.6.2 Hydrothermal mineral alteration

The distribution of the alteration minerals with regard to the order of occurrence, which represents the temperatures at which they were formed, is presented in Table 2. In HE-30, they occur as described below (Figure 6).

Oxides: These are formed from alteration of magnetite and oxidation of iron and chemical weathering of the rocks. Limonite and hematite were observed in HE-30. *Limonite* is yellowish to reddish brown of round shape with a dull metallic lustre and forms as surface coating as well as in fractures and vesicles. It was first seen at 114 m then occasionally throughout the well. It usually occurs together with siderite. *Hematite* is an opaque course crystalline of reddish brown to blackish colour, with shiny metallic lustre and occurs in between grains. It was seen at 250 m and towards the bottom of the well.

Carbonates are formed by reaction of carbonic acid with metals, weathering of metallic sulphides and alteration of other rock minerals (Saemundsson and Gunnlaugsson, 2010). Calcite and siderite were seen in HE-30. *Calcite* is the most common carbonate with an extreme birefringence and change in relief when it reacted with weak acids. It is white but coloured when it has impurities with dull lustre, rhomboidal cleavage or conchoidal fracture and occurs in many forms, for example as precipitation in amygdales, fissures and vein fillings. In HE-30, it was seen, evenly distributed, from the top to 1228 m with close association to the sulphides and other minerals. Platy calcite was seen at 108 m and thus representing boiling in the formation. *Siderite* is yellowish to reddish brown spherical or tabular crystals with perfect cleavage and vitreous lustre. It is found together with limonite and in veins or at intrusion margins. It was found from 114 m towards the bottom of the well.

Clays occurred as blueish/brown or greenish soft laminar very fine-grained particles with perfect cleavage. It forms as a result of alteration of the primary minerals. Smectite, chlorite and mixed layered clays (MLC) were observed throughout the well at different depths as seen from the binocular microscope and XRD analysis (Figure 6). *Smectite* is a greenish clay, formed as thin lining in amygdales and rock surfaces. It is brown in plain polarized light and green in crossed polar light. It was first observed from 116 to 772 m (Appendices I and II). *MLC* result from high-temperature hydrothermal alteration. They were seen from 456 to 876 m (Appendices I and II). There was a blue, unidentified, clay that was observed occasionally between 248 and 256 m. *Chlorite* has greenish to greenish brown fibre-like crystals that is found on rock surfaces, in vesicles and veins. It is associated with quartz, calcite and the high-temperature minerals. It was observed from 718 m (first appearance XRD analysis) (Appendices I and II) and from 754 m (first appearance in cuttings) to the bottom. It is indicative of temperatures ≥ 230°C (Table 2).

Zeolites are hydrated aluminium silicates which are colourless or white but coloured if containing impurities with variable cleavage, pearly or vitreous lustre and with uneven or conchoidal fractures. They are translucent or opaque. They form from precipitation and alteration in vesicles and veins at relatively low temperatures, below 200°C (Table 2) (Saemundsson and Gunnlaugsson, 2010). They occur in clusters in variable shapes and are associated with calcite, and sometimes quartz. They were observed from 100 m to 732 m. Chabazite, stilbite, scolecite, mesolite, thomsonite, garronite and phillipsite were seen in HE-30 from 100 to 732 m. *Chabazite* of white cubic shaped was found at 100 m (first appearance). It forms at around 50°C. *Scolecite* and *mesolite* are small elongated fibrous clustered crystals with a centred divergent radiation. They usually form at 70 – 80°C. Scolecite had thicker fibrous clustered crystals that were colourless or white and were first seen at 204 m. Mesolite occurred as white or greyish thin fibrous clustered crystals, which were seen at 220 m (first appearance). Stilbite was seen as thick tabular milky white crystals in bow tie form. It forms at around 90°C and was first seen at 312 m. *Thomsonite* occurred as flattened round milky white crystals and its first appearance was at 266 m depth and forms at around 100°C. *Phillipsite* occurred as thick blocky crystals that were colourless to white in colour. Its first appearance was at 346 m depth. Garronite was found in form of radiating concentric fractured milky white clustered crystals. It is a rare zeolite which forms at 120°C. It was seen at 348 m depth. *Wairakite* (>200°C) is found commonly in olivine tholeiites, in vesicles and fractures as transparent cubic crystal clusters with conchoidal fracture and has strong vitreous lustre with a conspicuous cross hatched twinning. It is a high temperature zeolite which usually occurs together with epidote, prehnite, calcite, quartz. It was first seen in 502 m in thin sections (Figures 6, 10 and 11) and at 534 m in cuttings.

TABLE 2: Temperature dependant minerals in high-temperature geothermal fields in Iceland (Kristmannsdóttir, 1979; Franzson, 1998)

Minerals	Min. temp. (°C)	Max. temp. (°C)
Zeolites	40	120
*Laumontite	120	180
*Wairakite	200	
Smectite		<200
**MLC	200	230
Chlorite	230	>300
Calcite	50-100	280-300
Quartz	180	>300
Prehnite	240	>300
Epidote	230-250	>300
Wollastonite	270	>300
Actinolite	280	>300
*Belong to the zeolite group **Mixed-layer clay		

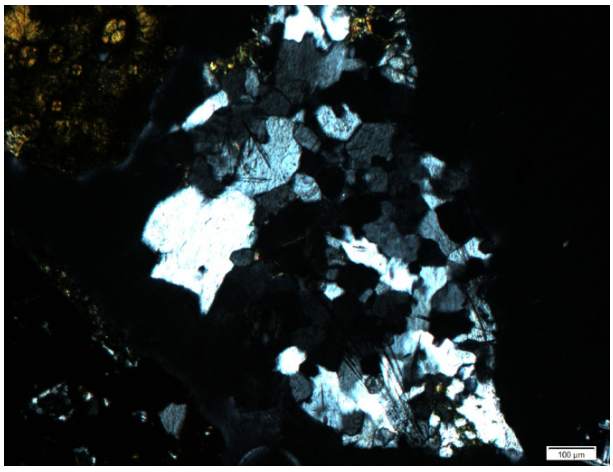

FIGURE 10: Wairakite at 502 m under crossed polars showed conspicuous cross hatched twinning in HE-30

Sulphides are found at margins of intrusions (Saemundsson and Gunnlaugsson, 2010). They sometimes occur in dykes and at geothermal springs in high-temperature areas (due to the presence of the H_2S in geothermal fields) and they are usually associated with calcite thus being indicator of permeability (Reyes, 2000; Saemundsson and Gunnlaugsson, 2010). In HE-30, pyrite and chalcopyrite were observed. *Pyrite* is cubic yellow with a strong metallic lustre and no cleavage. It is also formed from the deposition of hydrogen sulphide and/or from the alteration of oxides (Saemundsson and Gunnlaugsson, 2010). It was found as shiny coatings on fracture surfaces and in vesicles. It was seen from 128 m down to 790 m. *Chalcopyrite* forms by solidification of late magma gas-rich liquids (Saemundsson and Gunnlaugsson, 2010). It has indistinctive cleavage but is soft, yellow and tetragonal, though darker than pyrite. It was see from 790 m to the bottom.

Albite occurs as a transparent to translucent mineral as either a primary mineral (precipitation filling in vesicles) and/or an alteration of plagioclase. It has polysynthetic cleavage formed with low refractive index and is cloudy what differentiates it from quartz.

Silicates: Chalcedony is found in amygdales and cavities (as a coating) as white to grey translucent to opaque milky amorphous convex crystals (Saemundsson and Gunnlaugsson, 2010). The other colours are caused by oxidation. It is hexagonal with a greasy and waxy lustre and no cleavage. It was seen sparsely distributed from 314 to 788 m. *Quartz* (formed at 180°C) occurs in vesicles and fissures as hexagonal transparent, colourless, milky, greyish white crystals. It is deposited in cavities or as an alteration of chalcedony. It was well distributed in the well and was abundant in the bottom part of the well due to its temperature stability.

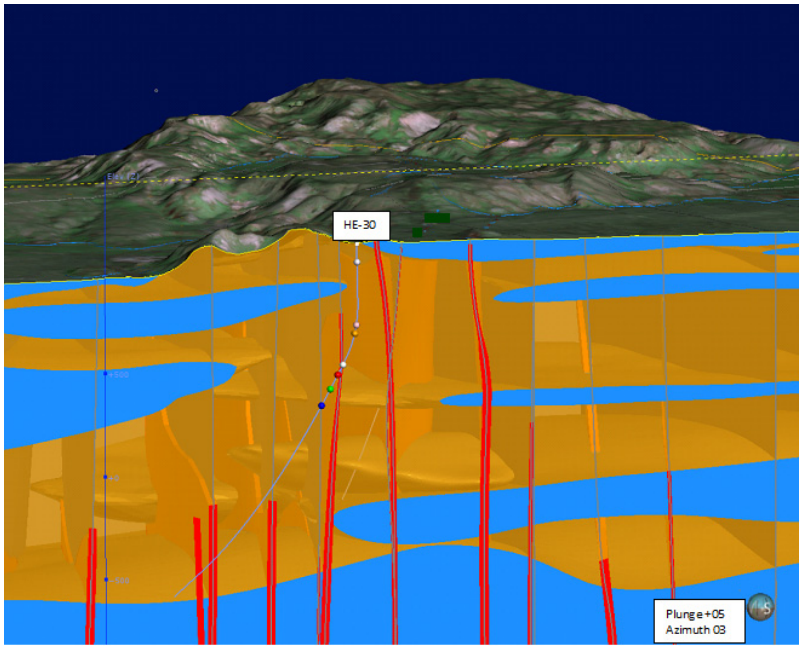

FIGURE 11: First appearance of alteration minerals in HE-30. Quartz (grey), wairakite (pink), prehnite (yellow), epidote (white and red), wollastonite (green), amphibole (blue)

Prehnite is made of white to grey rounded (orthorhombic) crystal clusters with distinct cleavage, irregular fracture and a strong birefringence which differentiates it from quartz. It was associated with the other high-temperature minerals, calcite, quartz, oxides and sulphides indicating temperatures ≥ 240°C. In HE-30, it was first seen at 654 m (Figures 6 and 11). *Epidote* are greenish yellow to pale green, translucent, microcrystalline (monoclinic) elongated prismatic fibrous crystals, with a high relief, vitreous lustre and unidirectional cleavage. It is an alteration product of feldspars, pyroxene and amphibole. It is stable at higher temperatures and indicates temperatures ≥ 240°C. It was widely distributed from 790 m (first appearance) (Figures 6 and 11) and well distributed towards the bottom. It occurred together with other high-temperature minerals like quartz, calcite, oxides and sulphides.

Wollastonite is found as very thin white fibres and occurs together with quartz, calcite andpidote. In He-30, it was associated with silicates, oxides, chalcopyrite, prehnite, epidote and actinolite at 844 m depth (first appearance, Figures 6 and 11) and at the bottom of well. It represents temperatures ≥ 270°C.

Amphiboles: Actinolite, which is a high-temperature mineral, was observed at 1014 m (first appearance), indicating ≥280°C. It occurred as thin, needle shaped, dark green crystals that resulted from the alteration of clinopyroxenes (Figures 6 and 11).

4.6.3 Alteration mineral zones

Hot hydrothermal fluids react with the host rocks forming hydrothermal minerals. There are a number of factors that influence the formation of alteration minerals such as permeability, temperature, duration of activity, rock composition, pressure, hydrothermal fluid composition and hydrology (Reyes, 2000; Marosvölgyi et al., 2010) resulting in mineral zonation with an increase of alteration with depth and

temperature in the well. In HE-30, 4 alteration zones (Figure 6 and Appendix I) were observed as shown below.

Unaltered zone (0 – 116 m): In this zone, there was no or slight oxidation and alteration which could be a result of interaction of run off or ground water with the host rock, thus magnetite, limonite, calcite and siderite occur.

Smectite – zeolite zone (116 – 456 m): In this zone there are zeolites (chabazite, stilbite, scolecite, phillipsite and mesolite) and low-temperature clays, smectite being the dominant one as seen from the XRD results (Appendices I and II). They represent a temperature range of 40 – 150°C. Other minerals in this zone include wairakite, chalcedony, quartz, hematite, limonite, siderite, calcite and pyrite.

Mixed layered clays zone (456 – 718 m): This zone is characterized by high-temperature clays Appendices I and II) representing temperatures from 150 – 230°C. They are associated with quartz, chalcedony, calcite, pyrite, zeolites and prehnite.

*Chlorite - epidote zone (718 – 1014 m): C*hlorite (Appendices I and II) and epidote became more evident in this zone representing a temperature ≥ 250°C. They are found together with prehnite, chalcopyrite and limonite.

Epidote – actinolite zone (1014 – 1328 m): Chlorite and epidote were dominant in this zone. They define temperatures ≥ 280°C. The rocks in this zone were greatly altered and the upper part was intensely fractured, with abundance of chlorite and epidote. At the bottom, there was less epidote and chlorite and no calcite. Wollastonite and actinolite were observed together with prehnite, quartz, limonite and siderite.

4.7 Vesicles, vein fillings and mineral deposition sequences

4.7.1 Vesicles and vein fillings

Veins and vesicles contribute greatly to porosity and permeability, which control the transportation and storage of fluids within the rocks. Due to different conditions of the rock and fluids, for example temperature, pressure, fluid composition and many others, alteration minerals are deposited and/or replace the primary minerals in fractures and vesicles resulting in deposition sequences of secondary minerals. Hydrothermal mineral deposition in geothermal fields is mostly controlled by temperature. The most common minerals that were found in the vesicles and veins in HE-30 were calcite, pyrite, chalcedony, quartz, zeolites, chlorite and epidote. Clay formed a thin layer lining the vesicles. In the cuttings, veins were observed at different depths (42 m, 60 m, and 76 m) in fine- to medium-grained crystalline basalt at 66, 203 – 264, 284 – 286, 328 – 330, 352 – 376, 386, and 420 m in basaltic tuff, at 728 and 1184 m in basaltic breccia, at 1130 – 1138, 1268, 1280 and 1326 – 1328 m in pillow basalt, at 1002 – 1024 m in basaltic tuff and fine- to medium-grained crystalline basalt, at 132 – 220 m in fine- to medium-grained crystalline basalt and basaltic breccia, at 738 – 892 and 1008 – 1072 m in basaltic tuff and basaltic breccia and at 434 – 707 m in basaltic tuff, basaltic breccia and fine- to medium-grained crystalline basalt (Figure 6). For example, in the petrographic analysis, a vein was observed in 1096 m depth (Figure 12).

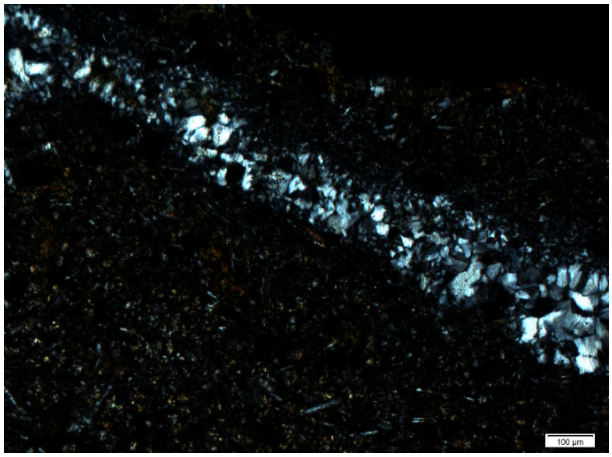

FIGURE 12: Vein filled with quartz in fine-grained crystalline basalt at 1096 m in HE-30

4.7.2 Mineral deposition sequence

Fractures and vesicles are conduits for the hydrothermal fluids, which react with the host rock causing deposition and replacement of minerals and wall rock alteration. This process determines the sequence of mineral deposition in relation to time and temperature. The sequences of mineral deposition (Table 3) in veins and vesicles in HE-30 were observed in the binocular and petrographic analyses, which included clay, calcite, quartz, zeolites, chlorite and epidote.

TABLE 3: Sequence of mineral deposition in HE-30

Depth (m)	Host rock	Sequence of mineral deposition
54	Basaltic tuff	clay → calcite
100	Basaltic tuff	calcite → chabazite
186	Basaltic tuff	calcite → stilbite
224	Basaltic tuff	smetite →quartz
292	Basaltic tuff	calcite →mesolite
372	Basaltic breccia	clay → calcite→ zeolites
434	Basaltic breccia	clay→ mesolite
502	Basaltic breccia	clay→ calcite
548	Fine -medium crystalline basalt	clay →calcite
584	Basaltic breccia	clay→ calcite →quartz
654	Fine -medium crystalline basalt	clay →calcite→ quartz
686	Fine -medium crystalline basalt	smetite →calcite
732	Fine -medium crystalline basalt	clay → calcite →zeolites
792	Basaltic breccia	clay → calcite
850	Basaltic breccia	clay → calcite
900	Basaltic tuff	clay → calcite→ chlorite
1034	Basaltic breccia	clay → chlorite→ calcite
1056	Basaltic breccia	clay →quartz
1184	Basaltic breccia	clay → quartz → epidote
1096	Basaltic breccia	clay → chlorite→ calcite
1236	Basaltic breccia	clay → chlorite →calcite
1278	Basaltic breccia	clay→ chlorite

4.8 Fluid inclusions

Microthermometric analysis from 17 fluid inclusions in two crystals (quartz at 758 – 762 m and calcite at 842 – 846 m) were conducted. Homogenization temperature (T_h) showed a range of 178 – 197, 202 – 220 and 254 – 255°C. The 254 – 255°C temperature range coincides to the estimated formation temperature at that depth range (758 – 762 m) which is around 250°C as seen in Figure 10, while the 178 – 197 and 202 – 220°C temperature ranges as well as the T_h at 842 – 846 m were low compared to the estimated formation temperature.

Comparison of alteration, fluid inclusion and formation temperatures

Fluid inclusion analysis, homogenization temperatures (T_h) at which the alteration minerals first appeared and the formation temperature were used to understand the thermal history of the system, showing if it was heating up, cooling or in equilibrium. Other factors have to be considered when interpreting the thermal history of the system, as there could be eruptive fissures or a magma chamber causing increased heating or a cold inflow leading to cooling of the system. The formation and alteration temperature are almost identical (Figure 8). Homogenization temperatures (T_h) being lower than formation and alteration temperatures could represent an old formation temperature (Figure 8). However, by comparing alteration temperature, formation temperature and the boiling point curve it is concluded that the system is presently in thermal equilibrium.

5. DISCUSSION

HE-30 is composed of alternating interglacial lavas and hyaloclastites, occasionally cut by intrusions, and the sequence is partly covered by postglacial lava flows. The alteration intensity and mineral deposition increases with depth (Figures 6 and 11). There were four alteration zones observed in HE-30, smectite- zeolite at 116 – 456 m, mixed layer clay at 456 – 718 m, chlorite- epidote at 718 – 1014 m and epidote – actinolite 1014 – 1328 m.

Faults, lithological boundaries and intrusions were the major cause of permeability in HE-30. Different sizes of feed-zones were seen at different depths in different lithologies from 0 to 1960 m in HE-30 as seen from circulation losses and temperature logs. Table 1 shows that the aquifers above 705 m were sealed off by casing and cementing the well with production casing.

Alteration and formation temperatures are almost identical and the alteration minaralogy indicates that the well temperature is > 250° C at 700 m depth.

The homogenization temperature (T_h) derived from the fluid inclusions is 178°C – 197°C, 202°C and 254°C -255°C in quartz crystal at 758 -762 m and 213°C - 220°C in calcite crystal at 842 – 846 m. It was lower than the estimated formation temperature which could indicate older alteration.

The objective of drilling HE-30 was achieved as seen in Figures 7 and 11, which show that the faults and the Reykjafell minigraben were intercepted. This resulted in a well with a productivity above average in the Hellisheidi geothermal field.

6. CONCLUSIONS

The main conclusions in this report are as follows:

- Hyaloclastites (basaltic tuff, basaltic breccia and pillow lavas) and fine- to medium-grained crystalline basalts are the major geological formations in HE-30.
- The intrusions were fine- to medium-grained crystalline basalts.
- Permeability is caused by faults, intrusives and lithological boundaries.
- Thirteen feed zones were found down to 1960 m depth.
- The sequence of mineral deposition is dependent on the rock type, permeability and temperature resulting in four alteration zones.
- The sequence of mineral deposition is dependent on the rock type, permeability and temperature.
- Hydrothermal alteration compared to formation temperature indicates that the system is in thermodynamic equilibrium.
- The low homogenization temperatures (T_h) could be representing old temperature conditions.

ACKNOWLEDGEMENTS

I am grateful to the management and staff of United Nations University Geothermal Training Programme (UNU-GTP) for sponsoring me and giving me the precious opportunity to undertake this training and the knowledge, especially Mr. Lúdvík S. Georgsson, Mr. Ingimar G. Haraldsson, Ms. Thórhildur Ísberg, Mr. Markús A.G. Wilde, and Mrs. Málfrídur Ómarsdóttir, who never stopped attending to me whenever I needed their assistance; the Icelandic GeoSurvey (ISOR) not forgetting Ms. Sveinborg H. Gunnarsdóttir, Mr. Bastien Poux, Mrs. Saeunn Halldórsdóttir, Mrs. Helga M. Helgadóttir and Dr. Hjalti Franzson for their technical assistance. Special thanks to my supervisor Dr. Björn S. Hardarson for his parental and generous technical guidance and support. I also thank Reykjavik Energy for allowing me to access HE-30 data.

I am grateful to my employer Ministry of Energy and Mineral Development - Directorate of Geological Survey and Mines (DGSM) for permitting me to attend this training. I am forever and greatly indebted to my God sent husband Mr. Timothy Sembatya for taking care of the children and for being supportive and understanding throughout this time, my sweet sister Dr. Justine N. Busingye for sacrificing

everything else whenever we needed you and my colleagues at DGSM for the overwhelming support. I thank my UNU fellows for your cooperation throughout the training.

Finally, I give God the glory for sustaining me and my family through this training.

REFERENCES

Árnason, K., 2007: *TEM resistivity surveys at the Hengill area 2006 and proposed experimental drilling by Eldborg.* ÍSOR – Iceland GeoSurvey, Reykjavík, report, ISOR-04001 (in Icelandic), 34 pp.

Bawasu, M.L., 2010: Borehole stratigraphy and alteration mineralogy of well HE-6, Hellisheidi, SW-Iceland. Report 9 in *Geothermal training in Iceland 2010*. UNU-GTP, Iceland, 65-90.

Björnsson, A., and Hersir, G.P., 1981: Geophysical reconnaissance study of the Hengill high temperature area, SW-Iceland. *Geothermal Resources Council, Transactions, 5*, 55-58.

Bodnar, R.J., 2003: Introduction to fluid inclusions, Analysis and Interpretation. *Mineral Association of Canada, Short Course Series 32*, 8 pp.

Franzson, H., 1998: Reservoir geology of the Nesjavellir high-temperature field in SW-Iceland. *Proceedings of the 19th Annual PNOC-EDC Geothermal Conference, Manila*, 13-20.

Franzson, H., Gunnlaugsson E., Árnason, K., Saemundsson, K., Steingrímsson, B., and Hardarson, B.S., 2010: The Hengill geothermal system, conceptual model and thermal evolution. *Proceedings of the World Geothermal Congress 2010, Bali, Indonesia,* 19 pp.

Gasperikova, E., Rosenkjaer, K.G., Árnason, K., Newman, A.G., and Lindsey, J.N., 2015: Resistivity characterization of Krafla and Hengill geothermal fields through 3D MT inverse modelling, *Geothermics, 57,* 246-257.

Gebrehiwot Mesfin, K., 2010: *Subsurface geology, hydrothermal alteration and geothermal model of northern Skardsmyrarfjall, Hellisheidi geothermal field.* University of Iceland, MSc thesis, UNU-GTP, report 5, 65 pp.

Gunnarsdóttir, S.H., 2012: *Geology and alteration of Mount. Reykjafell, Hellisheidi, Iceland*. University of Iceland, Reykjavík, MSc thesis (in Icelandic), 197 pp.

Haraldsdóttir, S., Franzson, H., and Árnason, K., 2015: Comparison of down hole data and surface resistivity data from S-Hengill, a high temperature geothermal field in SW-Iceland. *Proceedings of the World Geothermal Congress 2015, Melbourne, Australia*, 12 pp.

Hardarson, B.S., 2014: Geothermal exploration of the Hengill high temperature area. *Presented at Short course IX on exploration for geothermal resources 2014, organized by UNU-GTP, KenGen and GDC, Naivasha, Kenya*, UNU-GTP SC-19, 9 pp.

Hardarson, B.S., Fitton, J.G., Ellam, R.M. and Pringle, M.S, 1997: Rift relocation - a geochemical and geochronological investigation of a paleo-rift in northwest Iceland. *Earth Planet Science Letters, 153*, 181-196.

Hardarson, B.S., Franzson, H., Gudbrandsson, S., Pétursson, F., Sigurdsson, G., Kjartansson, O., Sigurdsson, Ó., Jónsson, P., Danielsen, P.E., and Brynleifsson, T., 2007a: *Hellisheidi – Well HE-30. Predrilling, Phase 1 and 2: Drilling for 22½" surface casing to 90 m, 18⅝" safety casing to 300 m and*

13⅜" production casing to 707 m depth. ÍSOR – Iceland GeoSurvey, Reykjavík, report ISOR/2007/033 (in Icelandic), 81 pp.

Hardarson, B.S., Júlíusson, E., Einarsson, G.M., Jónsson, S.S., and Gudbrandsson, S., 2007b*: Hellisheidi – Well HE-30. Phase 3: Drilling of production part from 707 m to 2318 m depth for a 9⅝" liner.* ÍSOR – Iceland GeoSurvey, Reykjavík, report ISOR/2007/037 (in Icelandic), 118 pp.

Hardarson, B.S., Kristinsson, S.G., Karlsdóttir, R., and Einarsson, G.M., 2015: Geothermal implications of rift zone mini-grabens. Geological and geophysical structure of the Reykjafell mini-graben, Hengill geothermal field, SW Iceland. *Proceedings of the World Geothermal Congress 2015, Melbourne, Australia,* 11 pp.

Helgadóttir, M.H., Hardarson, B.S., and Franzson, H., 2016: *Lectures notes on logging drill cuttings*. UNU-GTP, Iceland, unpublished lecture notes, 19 pp.

Kristmannsdóttir, H., 1979: Alteration of basaltic rocks by hydrothermal activity at 100-300°C. In: Mortland, M.M., and Farmer, V.C. (editors), *International Clay Conference 1978*. Elsevier Scientific Publishing Co., Amsterdam, 359-367.

Marosvölgyi, K., Kristmannsdóttir, H., and Lacasse, C., 2010: Retrograde alteration of basaltic rocks in the Theistareykir high-temperature geothermal field, North-Iceland. *Proceedings of the World Geothermal Congress 2010, Bali, Indonesia,* 9 pp.

Reyes, A.G., 2000: *Petrology and mineral alteration in hydrothermal systems: from diagenesis to volcanic catastrophes.* UNU-GTP, Iceland, report 18, 1998, 77 pp.

Saemundsson, K., 1979, Outline of the geology of Iceland, *Jökull, 29*, 7-28.

Saemundsson, K., and Gunnlaugsson, E., 2002: *Icelandic rocks and minerals*. Edda and Media Publishing, Reykjavík, Iceland, 233 pp.

Shepherd, T.J., Rankin, A.H., and Alderton, D.H.A., 1985: *Practical guide to fluid inclusion studies.* Blackie and Sons, Glasgow, UK, 239 pp.

Spichak, V.V., Zakharova, K.O., and Goidina. G.A., 2013: A new conceptual model of the Icelandic crust in the Hengill geothermal area based on the indirect electromagnetic geothermometry *J. Volcan. Geoth. Res. 257,* 99-112.

Steingrímsson, B, and Gudmundsson A., 2006: Geothermal borehole investigations during and after drilling. W*orkshop for decision makers on geothermal projects in Central America, organized by UNU-GTP and LaGeo in San Salvador, El Salvador, 2006,* 10 pp.

APPENDIX I: Details of XRD analysis of clay

Sample #	Depth (m)	d(001) OMH	d(001) GLY	d(001) HT	d(002)	Type	Other minerals
#01	58	-	-	-	-	-	
#02	116	13.81	15.93	10.04		sm	
#03	162	13.9	13.9	10.04		sm	
#04	218	13.98	13.98	10.04		sm	
#05	264	14.76	14.76	9.86		sm	
#06	322	13.6	13.6	10.1		sm	Å=9.1 zeol.?
#07	388	13.12	13.62	10		sm	Å=9.1 zeol.?
#08	456	30.91 / 13.24	30.91 / 13.87	9.97	7.2 HIT=0	MLC	Å=9.1 zeol.?
#09	512	13.13	13.78	9.98		sm	
#10	590	32.53 / 14.54	32.53 / 14.54	12.74	7.2 HIT=0	MLC	
#11	662	13.55	13.97	10.2	7.12 HIT=0	sm/MLC	Å=9.1 og 8.97 zeol.?
#12	718	14.34	14.34		7.23 HIT=0	Chl. unst.	
#13	772	15.14	15.85	10.79	7.29 HIT=0	sm/MLC	
#14	824	30.80 / 14.57	30.80 / 14.57	14.57	7.2 HIT=0	MLC	
#15	876	30.79 / 14.86	30.79 / 14.86		7.27 HIT=0	MLC	Å=7.75 ?
#16	926	14.57	14.57	14.57	7.19	Chl	
#17	992	14.76	14.76	14.76	7.22	Chl	Å=7.73 ?
#18	1040	14.6	14.6	14.6	7.2	Chl	Å=7.71?
#19	1140	14.65	14.65	14.65	7.22 HIT=0	Chl. unst.	
#20	1186	14.65	14.65	14.65	7.20 HIT=0	Chl. ill	Å=10.05 illite
#21	1244	14.43	14.43	14.43	7.15 HIT=0	Chl. unst.	
#22	1282	14.81	14.81	14.81	7.26 HIT=0	Chl. unst.	

Appendix II: Graphs from XRD analysis of samples at different depths in HE-30

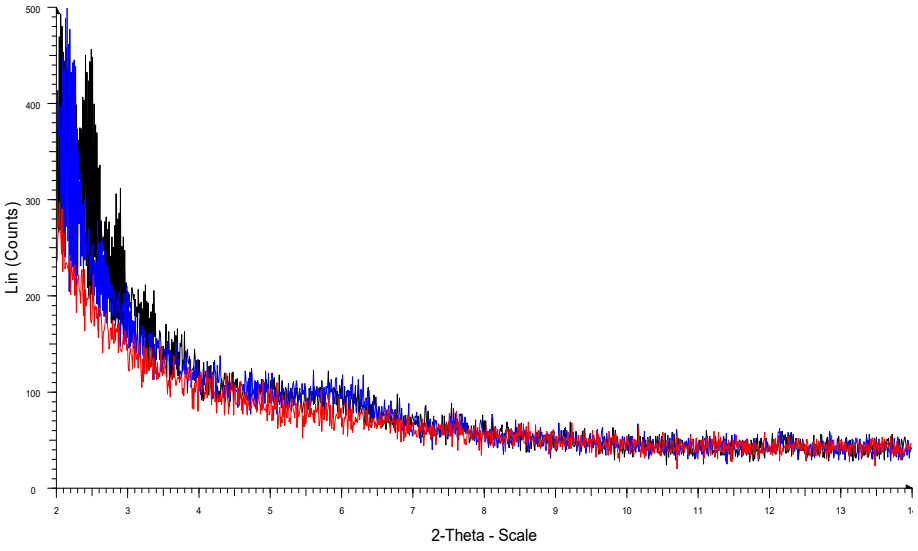

FIGURE 1: HE-30 at 58 m

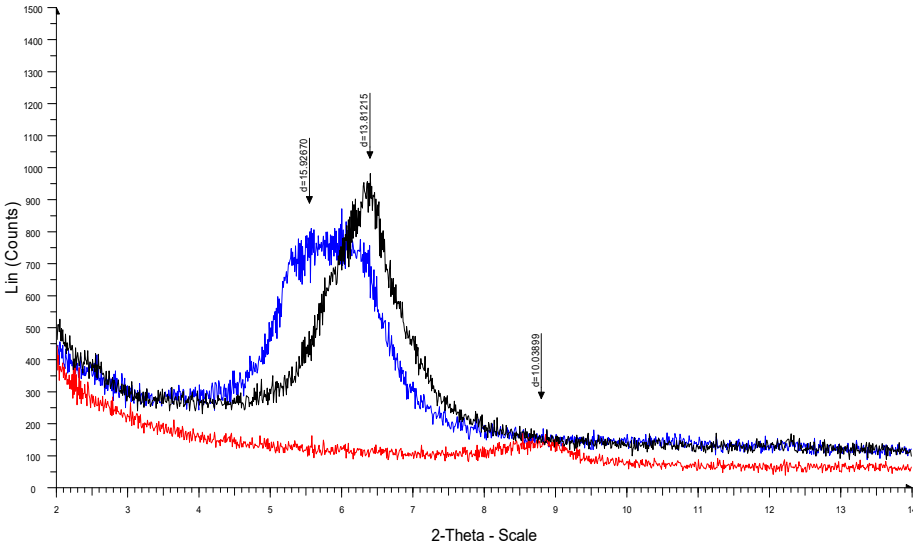

FIGURE 2: HE-30 at 116 m

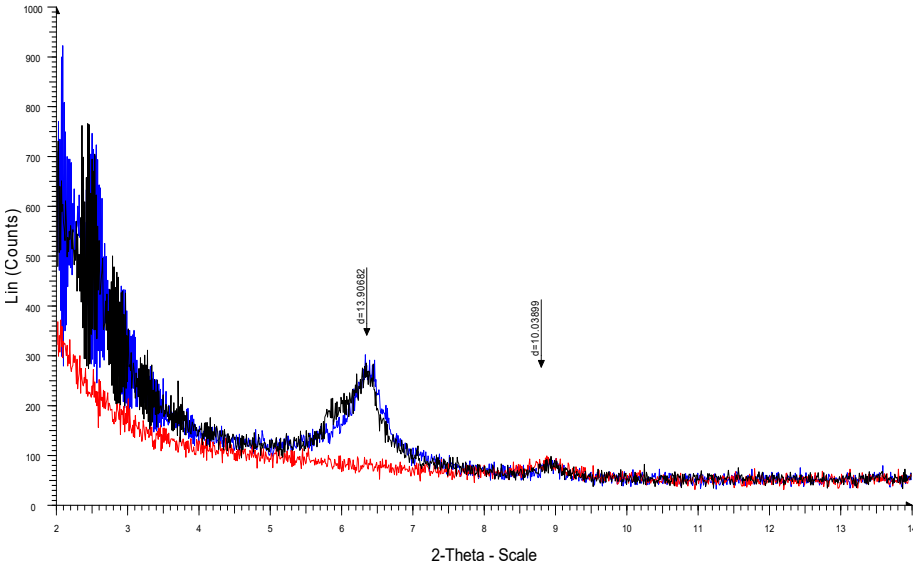

FIGURE 3: HE-30 at 162 m

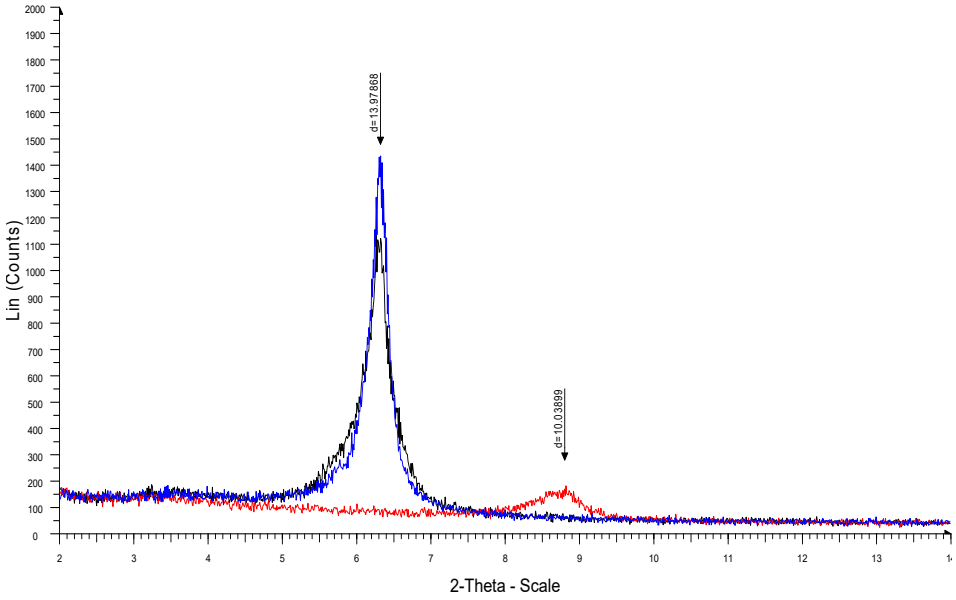

FIGURE 4: HE-30 at 218 m

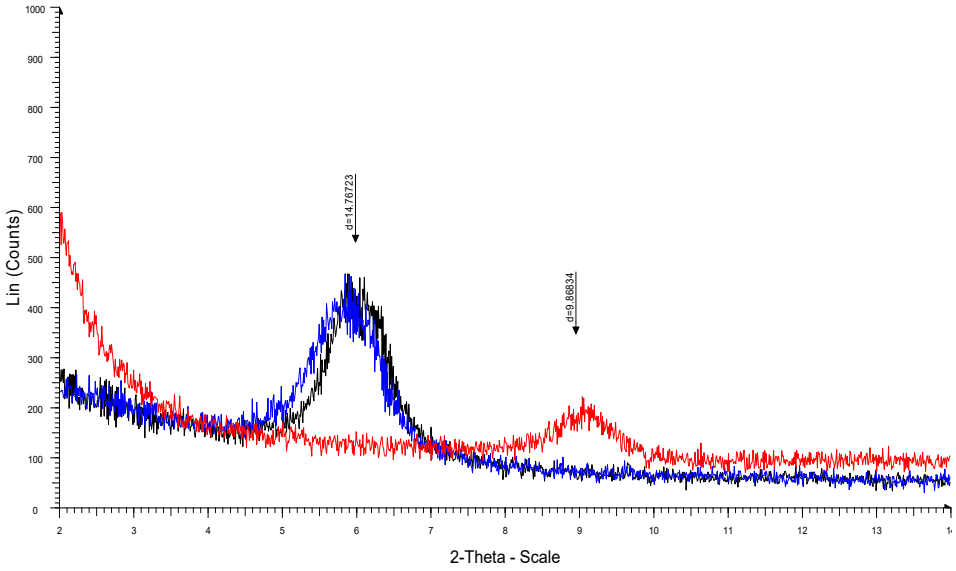

FIGURE 5: HE-30 at 264 m

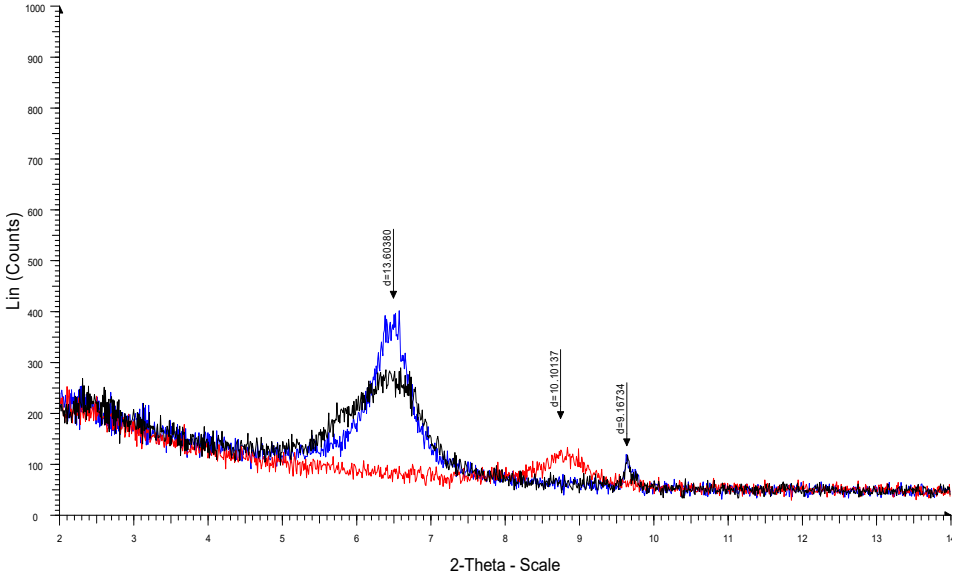

FIGURE 6: HE-30 at 322 m

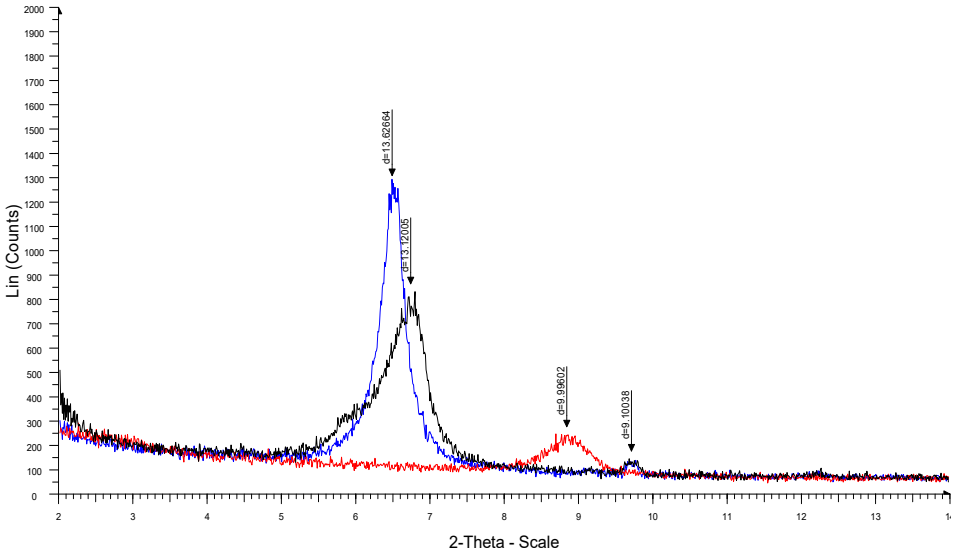

FIGURE 7: HE-30 at 388 m

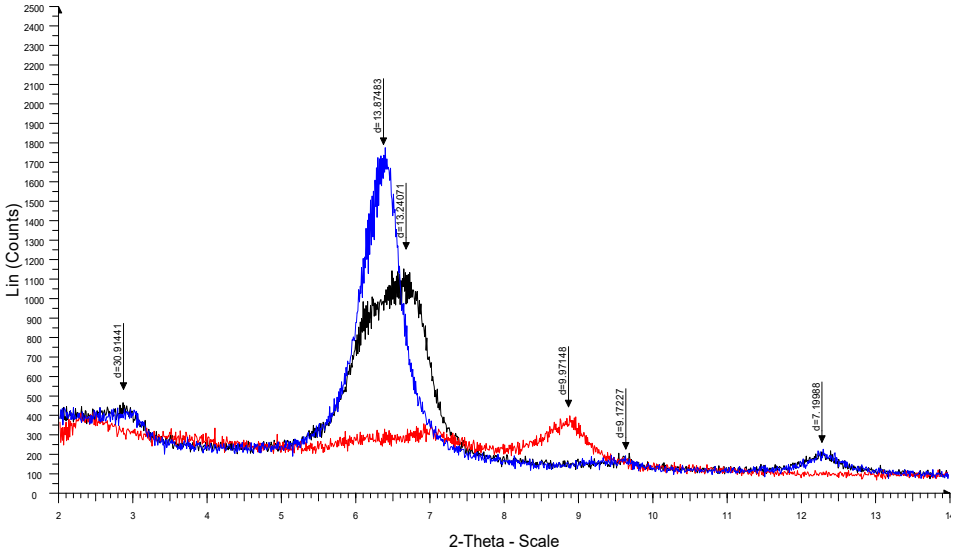

FIGURE 8: HE-30 at 456 m

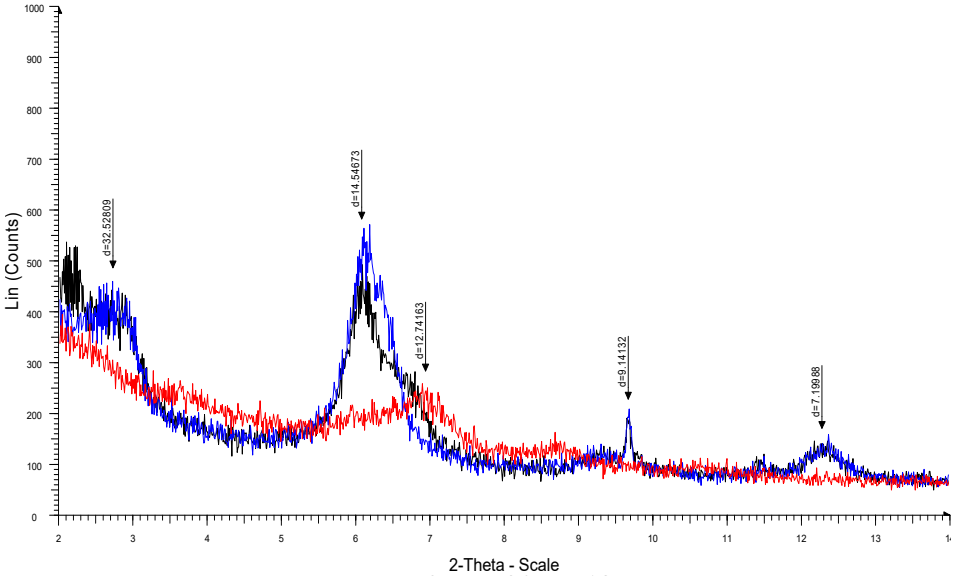

FIGURE 9: HE-30 at 512 m

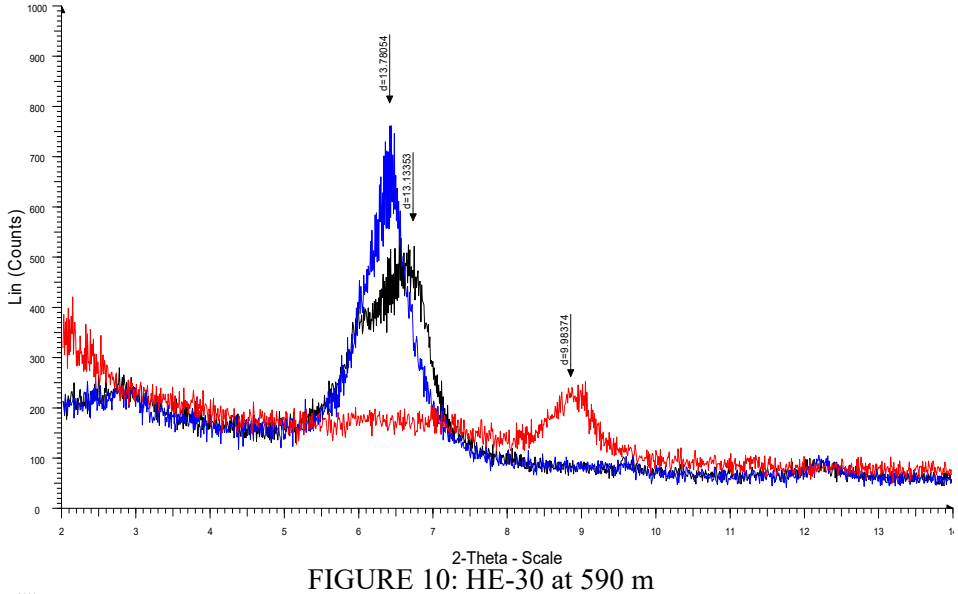

FIGURE 10: HE-30 at 590 m

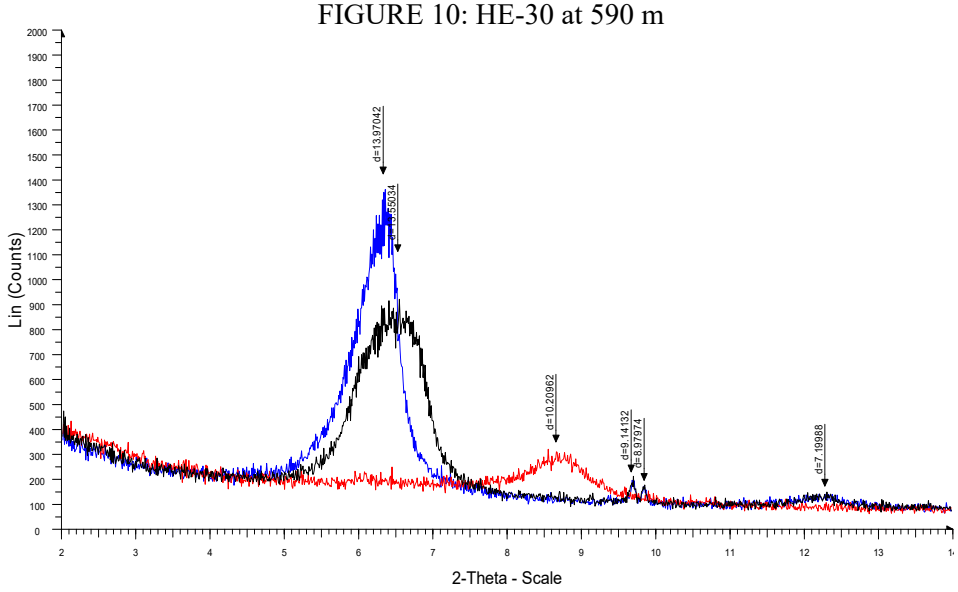

FIGURE 11: HE-30 at 662 m

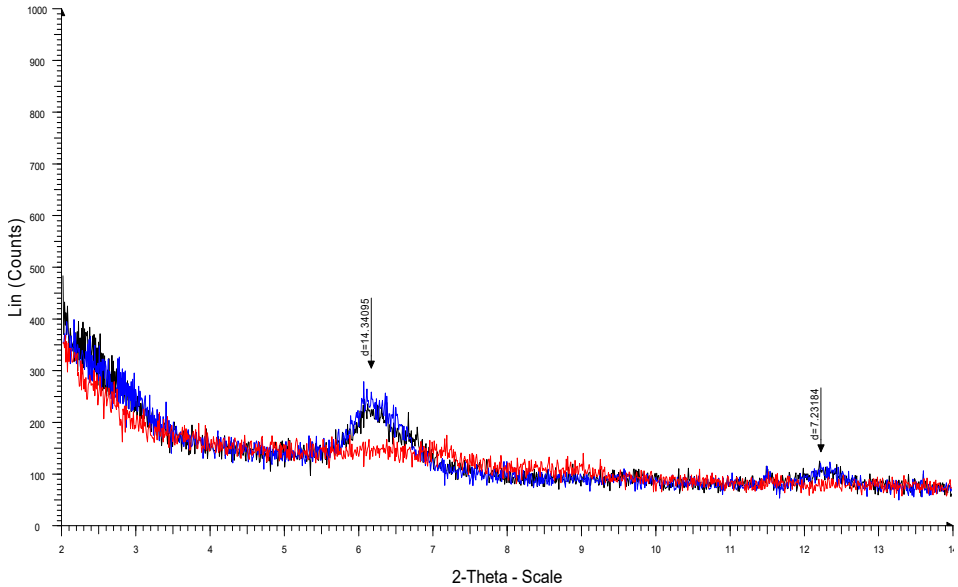

FIGURE 12: HE-30 at 718 m

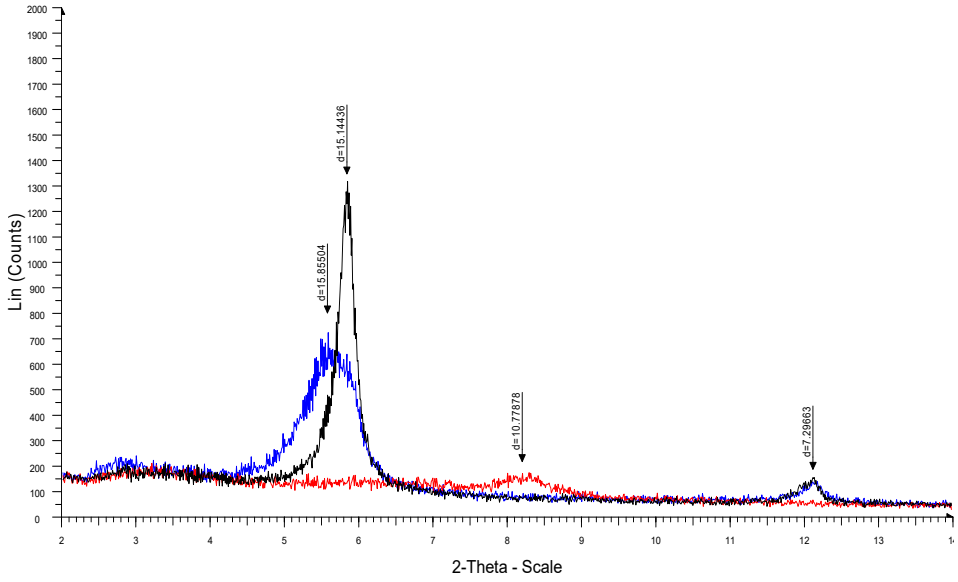

FIGURE 13: HE-30 at 772 m

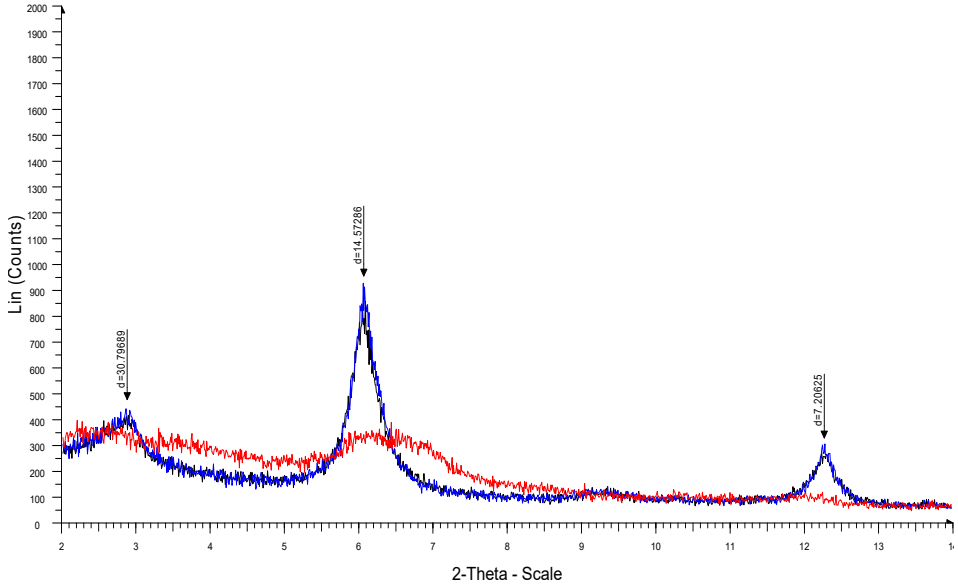

FIGURE 14: HE-30 at 824 m

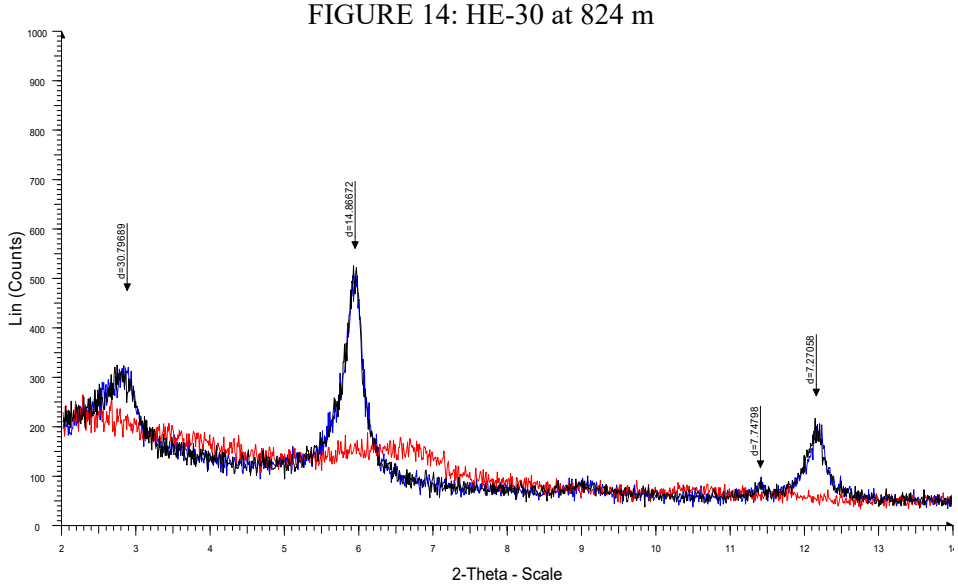

FIGURE 15: HE-30 at 876 m

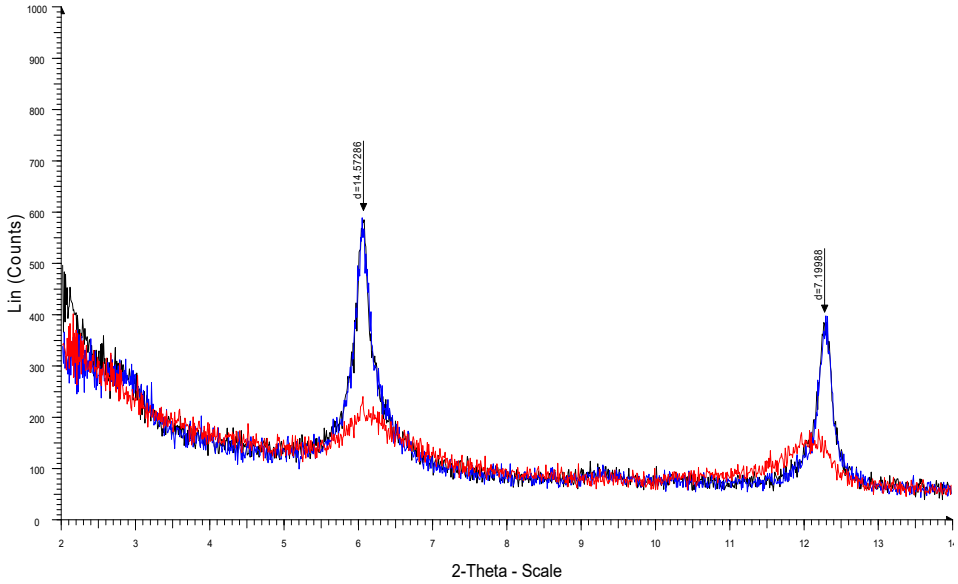

FIGURE 16: HE-30 at 926 m

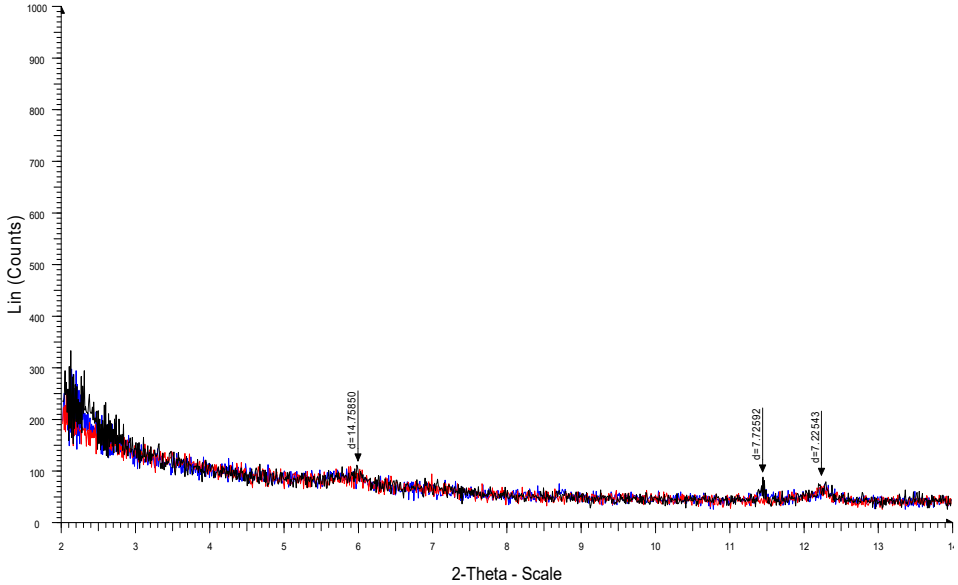

FIGURE 17: HE-30 at 992 m

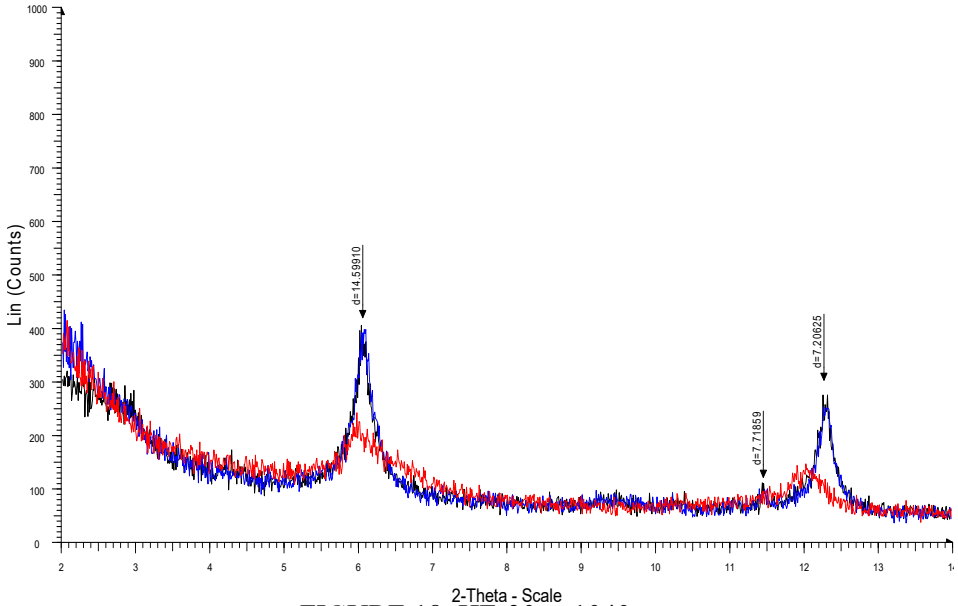

FIGURE 18: HE-30 at 1040 m

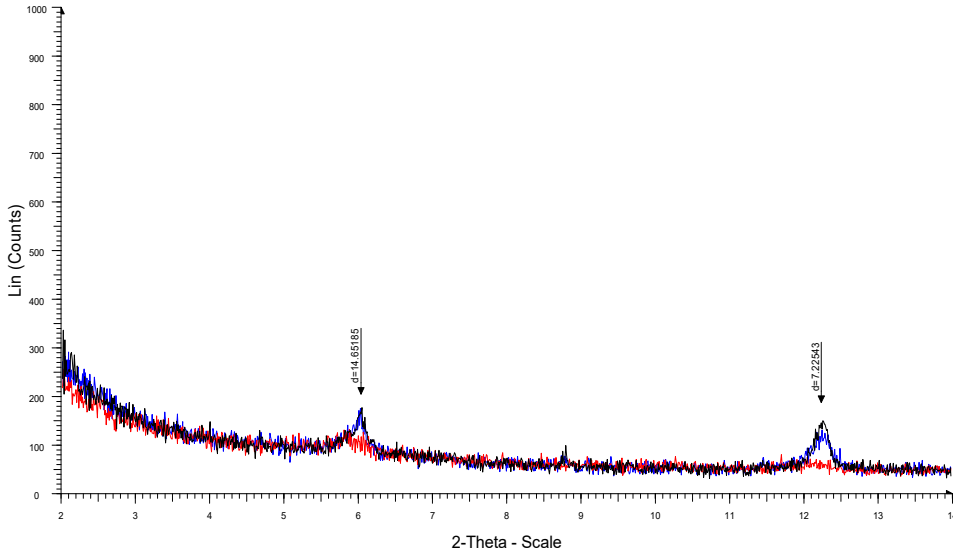

FIGURE 19: HE-30 at 1140 m

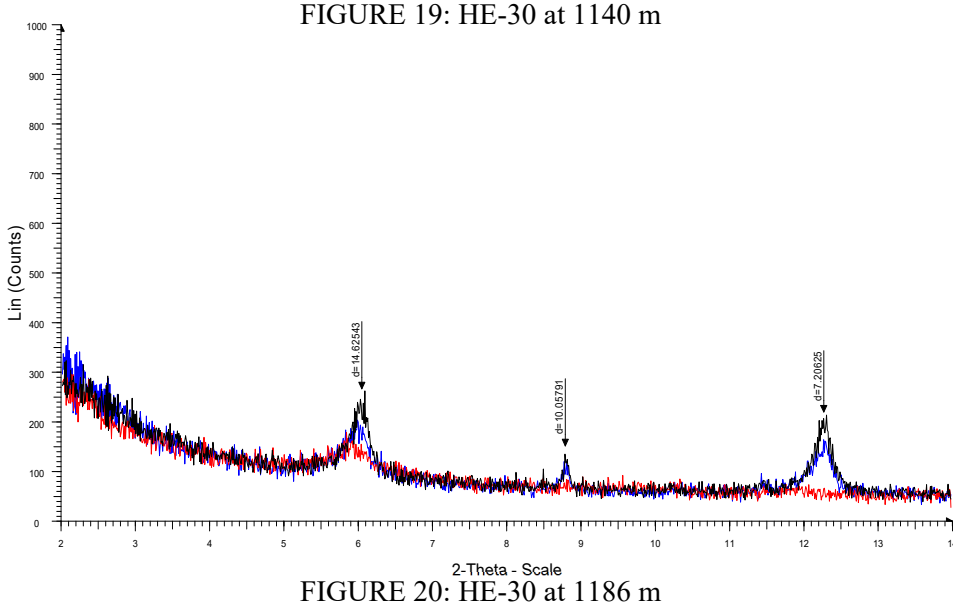

FIGURE 20: HE-30 at 1186 m

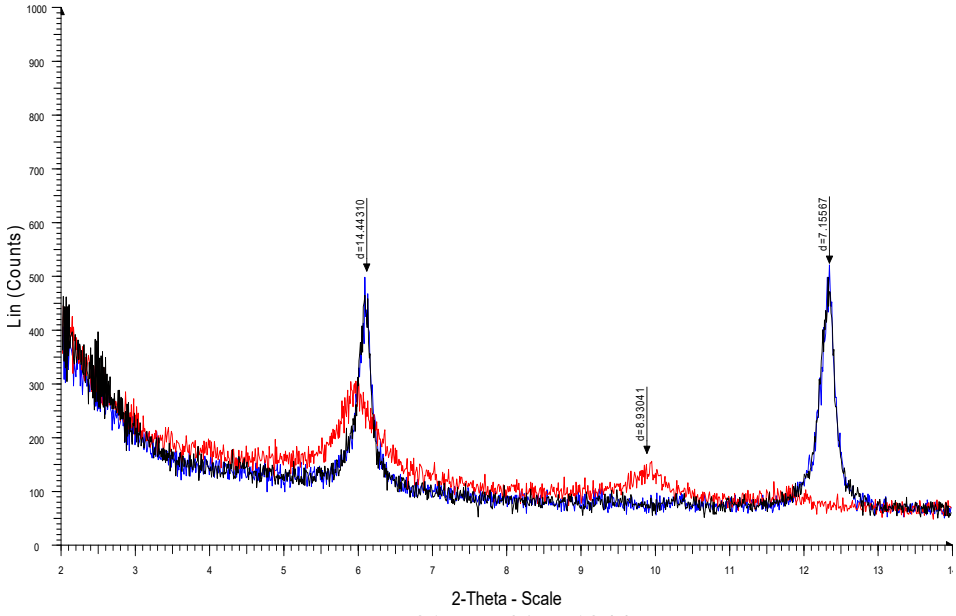

FIGURE 21: HE-30 at 1244 m

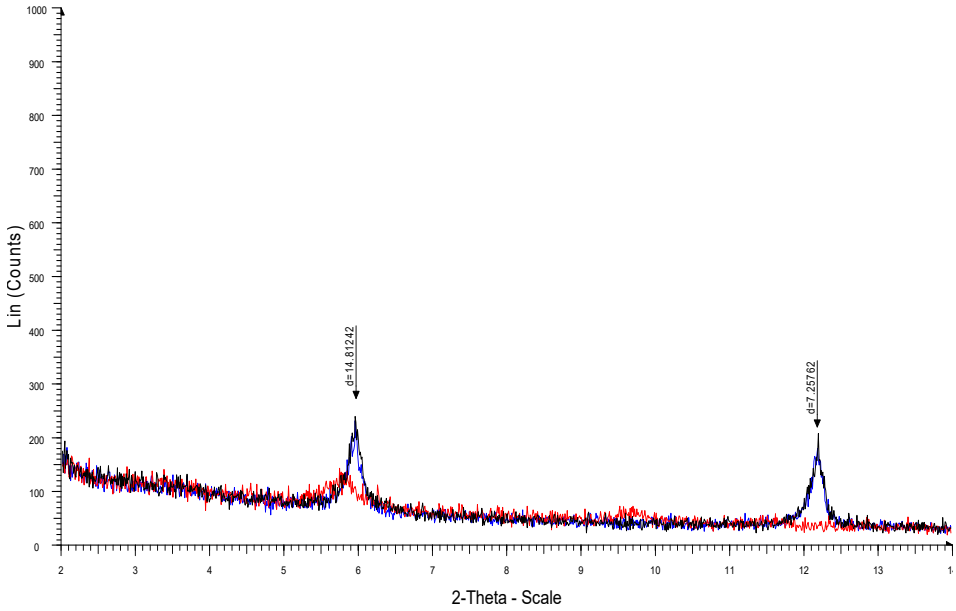

FIGURE 21: HE-30 at 1282 m